

1 **Distinct cellular expression and subcellular localization of Kv2 voltage-gated K<sup>+</sup> channel subtypes in**  
2 **dorsal root ganglion neurons conserved between mice and humans**

3

4 Robert G. Stewart<sup>1</sup>, Miriam Camacena<sup>1</sup>, Bryan A. Copits<sup>2</sup>, Jon T. Sack<sup>1,3</sup>

5

6 **Affiliations:**

7 <sup>1</sup> Department of Physiology and Membrane Biology, University of California Davis,

8 Davis, CA 95616, USA.

9 <sup>2</sup> Washington University Pain Center, Washington University School of Medicine, St. Louis, MO 63110,

10 USA; Department of Anesthesiology, Washington University School of Medicine, St. Louis, MO 63110,

11 USA.

12 <sup>3</sup> Department of Anesthesiology and Pain Medicine, University of California Davis,

13 Davis, CA 95616, USA.

14 **Corresponding author email:** jsack@ucdavis.edu

15 **Number of figures:** 10

16 **Number of supplemental figures:** 15

17 **Number of tables:** 2

18 **Conflict of interest statement:** The authors declare no competing conflicts of interest.

19 **Data availability:** The data that support the findings of this study are available upon request from the

20 authors. Code used to analyze this data in ImageJ and R is available at <https://github.com/SackLab/DRG->

21 [Image-Processing](#)

22 **Running Title:** Kv2 localization in DRG neurons

23 **Keywords:** Dorsal root ganglion, Voltage gated ion channels, Kv2.1, Kv2.2, Somatosensory neurons

24 **Acknowledgments:**

25 We thank James S. Trimmer (University of California, Davis) for generous provision of antibodies,  
26 numerous discussions, and feedback on the manuscript. We thank Michael Ferns (University of  
27 California, Davis) for feedback on the manuscript. We thank the human tissue donors and their families  
28 for their generous donations to science. We thank Jiwon Yi, Zack Bertels, Maria Payne, and Jon Lemen  
29 for performing hDRG extractions. GxTX was synthesized at the Molecular Foundry of the U.S.  
30 Department of Energy under contract DE-AC02-05CH11231. This research was supported by U.S.  
31 National Institutes of Health grant R01NS096317 to J.T. Sack and the University of California, Davis.

32 **Author contributions:** R. G. Stewart: Conceptualization, formal analysis, investigation, methodology,  
33 visualization, writing-original draft, writing-reviewing and editing. M. Camacena: investigation. B. A.  
34 Copits investigation, writing-reviewing and editing. J.T. Sack: Conceptualization, formal analysis, funding  
35 acquisition, investigation, methodology, project administration, supervision, visualization, writing-  
36 original draft, writing-reviewing and editing.

37 **ABSTRACT**

38

39 The distinct organization of Kv2 voltage-gated potassium channels on and near the cell body of brain  
40 neurons enables their regulation of action potentials and specialized membrane contact sites.

41 Somatosensory neurons have a pseudounipolar morphology and transmit action potentials from

42 peripheral nerve endings through axons that bifurcate to the spinal cord and the cell body within ganglia

43 including the dorsal root ganglia (DRG). Kv2 channels regulate action potentials in somatosensory

44 neurons, yet little is known about where Kv2 channels are located. Here we define the cellular and

45 subcellular localization of the Kv2 paralogs, Kv2.1 and Kv2.2, in DRG somatosensory neurons with a

46 panel of antibodies, cell markers, and genetically modified mice. We find that relative to spinal cord

47 neurons, DRG neurons have similar levels of detectable Kv2.1, and higher levels of Kv2.2. In older mice,

48 detectable Kv2.2 remains similar while detectable Kv2.1 decreases. Both Kv2 subtypes adopt clustered

49 subcellular patterns that are distinct from central neurons. Most DRG neurons co-express Kv2.1 and

50 Kv2.2, although neuron subpopulations show preferential expression of Kv2.1 or Kv2.2. We find that Kv2

51 protein expression and subcellular localization is similar between mouse and human DRG neurons. We

52 conclude that the organization of both Kv2 channels is consistent with physiological roles in the somata

53 and stem axons of DRG neurons. The general prevalence of Kv2.2 in DRG as compared to central

54 neurons and the enrichment of Kv2.2 relative to detectable Kv2.1, in older mice, proprioceptors, and

55 axons suggest more widespread roles for Kv2.2 in DRG neurons.

56 **Significance statement**

57

58 The subcellular distribution of Kv2 voltage-gated potassium channels enable compartment-  
59 specific modulation of membrane excitability and organization of membrane contact sites. Here  
60 we identify subcellular distributions of the Kv2 paralogs, Kv2.1 and Kv2.2, in somatosensory  
61 neurons that bear similarities to and distinctions from central neurons. The distribution of Kv2  
62 channels is similar in mouse and human somatosensory neurons. These results identify unique  
63 locations of Kv2 channels in somatosensory neurons that could enable roles in sensory  
64 information processing.

65 **INTRODUCTION**

66

67 The subcellular localization of voltage-gated ion channels determines how electrical signals are  
68 propagated. The two members of the Kv2 family of voltage gated potassium channels, Kv2.1 and Kv2.2,  
69 are important for modulating electrical signals in mammalian somatosensory neurons (Bocksteins et al.,  
70 2009; Lee et al., 2020; Sun et al., 2022; Tsantoulas et al., 2014; Zheng et al., 2019), yet little is known  
71 about where Kv2 channels are localized in these neurons. In central neurons, Kv2 channels are  
72 sequestered to specific subcellular regions and identification of where these channels are has helped  
73 elucidate their functional roles (Bishop et al., 2015; Du, Tao-Cheng, Zerfas, & McBain, 1998; Irie, 2021;  
74 Jensen et al., 2017; Johnson et al., 2018; Kihira, Hermanstynne, & Misonou, 2010; Kirmiz, Vierra, Palacio,  
75 & Trimmer, 2018; Misonou, Mohapatra, Menegola, & Trimmer, 2005; Muennich & Fyffe, 2004; Romer et  
76 al., 2014; Scannevin, Murakoshi, Rhodes, & Trimmer, 1996; Trimmer, 1991; Vierra, O'Dwyer,  
77 Matsumoto, Santana, & Trimmer, 2021). Establishing where Kv2 channels are in somatosensory neurons  
78 likewise identifies sites where they could function.

79

80 Among vertebrates, the Kv2 family contains two conserved paralogs, Kv2.1 and Kv2.2, which can  
81 assemble into homo- or hetero-tetramers to form voltage gated K<sup>+</sup> channels (Blaine & Ribera, 1998;  
82 Kihira et al., 2010). In central neurons, Kv2.1 and Kv2.2 channels have unique cellular expression,  
83 subcellular localization, and show distinct physiological roles (Bishop et al., 2015; Newkirk et al., 2022).  
84 Among cortical neuron types, Kv2.1 is more broadly distributed than Kv2.2 (Bishop et al., 2015). Little is  
85 known of how Kv2.1 or Kv2.2 channels are distributed among somatosensory neuron subtypes. In  
86 central neurons, Kv2.1 and Kv2.2 channels localize in clusters on the cell soma, proximal dendrites, and  
87 axon initial segment (Bishop et al., 2015; King, Manning, & Trimmer, 2014; Sarmiere, Weigle, & Tamkun,  
88 2008; Scannevin et al., 1996; Trimmer, 1991). Clustered Kv2 channels form endoplasmic reticulum-

89 plasma membrane junctions (Johnson et al., 2018; Kirmiz et al., 2018), where they perform  
90 nonconducting functions which include mediating coupling of L-type calcium channels to ryanodine  
91 receptors (Vierra et al., 2021), and Ca<sup>2+</sup> uptake (Panzera et al., 2022). In somatosensory neurons it  
92 remains unknown whether Kv2 channels form organized structures or are localized to specific  
93 subcellular compartments. Identifying if channel expression is specific to neuron subtypes and within  
94 specific subcellular domains could indicate whether Kv2.1 and Kv2.2 channels also have distinct  
95 physiological roles in somatosensory neurons.

96

97 Kv2 channels are expressed and play important functional roles in DRG. Kv2 transcripts have been  
98 detected in all classes of DRG neurons with a notable absence of Kv2.1 mRNA in proprioceptors (Usoskin  
99 et al., 2015; Wangzhou et al., 2020; Zheng et al., 2019). Presence of Kv2.1 protein in DRG of mice and  
100 rats has been identified by western blot and immunohistochemistry respectively (Sun et al., 2022;  
101 Tsantoulas et al., 2012). Pharmacological inhibition of Kv2 channels enhances rat DRG neuron  
102 responsiveness to sustained inputs (Tsantoulas et al., 2014). Kv2 conductances have been identified in  
103 several mouse DRG neuron subtypes (Bocksteins et al., 2009; Regnier, Bocksteins, Van de Vijver,  
104 Snyders, & van Bogaert, 2016; Zheng et al., 2019). Kv2 channels have also been implicated in  
105 nociception. Kv2.1 and Kv2.2 mRNA transcript levels are decreased after peripheral axotomy of rat DRG  
106 neurons (Tsantoulas et al., 2014). Suppression of Kv2.1 transcription by the epigenetic factor Cdy1 is  
107 implicated in regulating pain sensation (Sun et al., 2022). A missing piece of the puzzle of how Kv2  
108 channels are involved in somatosensory neuron function is the location of the channels themselves.  
109 Here we use antibodies against Kv2.1 and Kv2.2 to define their cellular expression and subcellular  
110 localization in DRG neurons of both mice and humans.

111 **MATERIALS AND METHODS**

112

113 ***Mice***

114 This study was approved by the UC Davis Institutional Animal Care and Use Committee and conforms to  
115 guidelines established by the NIH. Mice were maintained on a 12 h light/dark cycle, and food and water  
116 was provided *ad libitum*. Kv2.1 KO and Kv2.2 KO mice were from breeding Kv2.1+/- or Kv2.2+/-  
117 heterozygous mice such that WT mice were from breeding pairs that generated KO mice. Kv2.1 and Kv2.2  
118 DKO mice were generated from breeding Kv2.1+/- heterozygous and Kv2.2-/- homozygous mice. WT  
119 controls for Kv2.1/Kv2.2 DKO experiments were C57BL/6J mice purchased from Jackson Laboratory (stock  
120 #000664). The *PV<sup>Ai14</sup>* mouse line was a generous gift from Dr. Theanne Griffith (University of California  
121 Davis, Davis CA) and were a cross of *Rosa26<sup>Ai14</sup>* (stock #007914, MGI: J:155793) and *PVcre* (stock #008069,  
122 MGI:J: 100886) mice. The *MrgprD<sup>GFP</sup>* mouse line was a generous gift from Dr. David Ginty (Harvard  
123 University, Boston MA) (MGI: 3521853). Detailed information about the genotype, age, sex and level of  
124 spinal column of mice used in each figure can be found in Table 1.

125

126 ***Human Tissue Collection***

127 Human DRG were obtained in collaboration with Mid-America Transplant (St. Louis, MO) from three  
128 donors. Donor #1 was a 59-year-old Caucasian male and the DRG was from the 2<sup>nd</sup> lumbar region (cause  
129 of death: anoxia/stroke). Donor #2 was a 59-year-old black male and the DRG was from the 3<sup>rd</sup> lumbar  
130 region (cause of death: hemorrhagic stroke). Donor #3 was a 58-year-old Caucasian female and the DRG  
131 was from the 3<sup>rd</sup> lumbar region (cause of death: cerebrovascular/stroke). DRG were extracted less than  
132 2 hours after aortic cross clamp and transported to the lab where they were dissected to remove the  
133 dura, embedded in Optimal Cutting Temperature (OCT) compound, snap frozen, and stored at -80 °C

134 until use (Valtcheva et al., 2016). Human DRG were obtained from organ donors with full legal consent  
135 for use of tissue for research in compliance with procedures approved by Mid-America Transplant.

136

### 137 ***Tissue Preparation***

138 Mice were briefly anesthetized with 3-5% isoflurane and then decapitated. The spinal column was  
139 dissected, and excess muscle tissue removed. The spinal column was then bisected in the middle of the  
140 L1 vertebrae identified by the 13<sup>th</sup> rib and drop fixed for 1 hour in ice cold PFA: 4% formaldehyde  
141 prepared fresh from paraformaldehyde in 0.1 M phosphate buffer (PB) pH adjusted to 7.4 with NaOH.  
142 0.1 M PB buffer was diluted from a 0.4 M PB stock solution that was made by diluting 91.37 g of  
143 Na<sub>2</sub>H<sub>2</sub>PO<sub>4</sub> and 20.98 g of Na<sub>2</sub>H<sub>2</sub>PO<sub>4</sub> • H<sub>2</sub>O in 2 liters of milliQ water. The relatively short fixation period  
144 was chosen because a longer fixation period increased the off target secondary antibody  
145 immunofluorescence from mouse isotype secondary antibodies (Supplemental Figure 1). The spine was  
146 washed 3× for 10 min each wash in PB and cryoprotected at 4 °C in 30% sucrose in PB for 24 hours. The  
147 spine was cut into sections containing two vertebra per sample which were frozen in OCT (Fisher  
148 cat#4585) and stored at -80 °C until sectioning. Vertebrae position relative to the 13<sup>th</sup> rib was recorded  
149 for each frozen sample to determine the specific vertebrae position in the spinal cord. Samples were cut  
150 into 30 µm sections on a freezing stage sliding microtome and were collected on Colorfrost Plus  
151 microscope slides (Fisher cat#12-550-19). Slides were stored at -20 °C or immediately used for multiplex  
152 immunofluorescence labeling.

153

154 Human DRG were cut into 30 µm sections on a freezing stage sliding microtome and were collected on  
155 Colorfrost Plus microscope slides. Sections were briefly thawed to adhere to the slide but were  
156 immediately returned to the cryostat kept at -20 °C. Slides were removed from the cryostat and  
157 immediately transferred to freshly made 4% PFA pH 7.4 for 10 minutes. Slides were then placed in PB

158 solution for 10 minutes and immediately used for multiplex immunofluorescence labeling. Attempts at  
159 immunolabeling Kv2 channels in human DRG tissue that was fixed in 4% PFA for 24 hours were not  
160 successful.

161

### 162 ***Neuron Cell Culture***

163 Cervical, thoracic and lumbar DRGs were harvested from mice and transferred to Hank's buffered saline  
164 solution (HBSS) (Invitrogen). Ganglia were treated with collagenase (2 mg/ml; Type P, Sigma-Aldrich) in  
165 HBSS for 15 min at 37°C followed by 0.05% Trypsin-EDTA (Gibco) for 2.5 min with gentle rotation. Trypsin  
166 was neutralized with culture media (MEM, with L-glutamine, Phenol Red, without sodium pyruvate)  
167 supplemented with 10% horse serum (heat-inactivated; Gibco), 10 U/ml penicillin, 10 µg/ml streptomycin,  
168 MEM vitamin solution (Gibco), and B-27 supplement (Gibco). Serum-containing media was decanted and  
169 neurons were triturated using a fire-polished Pasteur pipette in MEM culture media containing the  
170 supplements listed above. Neurons were plated on laminin-treated (0.05 mg/ml, Sigma-Aldrich) 35 mm  
171 glass bottom dishes (MatTek cat#P35G-1.5-7-C). Neurons were then incubated at 37°C in 5% CO<sub>2</sub>. Neurons  
172 were used for imaging experiments within 24 hours after plating.

173

### 174 ***Labeling Endogenous Kv2 in live cultured DRG neurons***

175 Plates were removed from 37°C incubator 24 hours after plating. Neurons were washed once with 1 mL  
176 neuronal external (NE) solution (3.5 KCl, 155 NaCl, 10 HEPES, 1.5 CaCl<sub>2</sub>, and 1 MgCl<sub>2</sub>, 10 mM glucose  
177 adjusted to pH 7.4 with NaOH). Neurons were then incubated with NE solution supplemented with 1%  
178 BSA for 5 minutes. Neurons were then washed once with NE solution and incubated in 5 µg/mL wheat  
179 germ agglutinin conjugated to Alexa Fluor 405 (Biotium cat#29028-1) diluted in NE solution for 2.5  
180 minutes. Neurons were washed twice with NE solution and imaged. NE solution was removed and then  
181 neurons were incubated for 10 minutes in 100 nM GxTX-594 prepared as described (Thapa et al., 2021).

182 Neurons were then washed three times in NE solution and imaged again. The temperature of the  
183 imaging chamber was 25 °C throughout the experiment. Experimenter was blinded to which culture  
184 dishes contained DRG neurons from either WT or Kv2.1/Kv2.2 double knockout mice throughout the  
185 experiment and image analysis.

186

### 187 ***Immunohistochemistry***

188 A hydrophobic barrier was drawn around tissue sections mounted on slides as described above using a  
189 hydrophobic barrier pen (Scientific Device cat#9804-02). Sections were incubated in 4% milk, 0.1 M  
190 phosphate buffer (PB) and 0.2% Triton X-100 (vehicle) for 1 hour. Sections were then incubated in  
191 vehicle containing 0.1 mg/mL IgG F(ab) polyclonal IgG antibody (Abcam cat#ab6668) for 1 hour. We  
192 determined that a concentration of 0.1 mg/mL maximally blocked off-target secondary antibody labeling  
193 when using isotype-specific anti-mouse secondary antibodies (Supplemental Figure 2). Sections were  
194 washed 3× for 5 min each in vehicle and then incubated in vehicle containing primary antibodies for 1  
195 hour. Primary antibodies and concentrations used are listed in Table 2. Sections were then washed 3×  
196 for 5 min each in vehicle and then incubated in vehicle containing IgG-subclass-specific secondary Abs  
197 for one hour (Thermo Fisher). Sections were then washed 3× for 5 min each in PB and mounted with  
198 Prolong Gold (Thermo Fisher cat#P36930) and Deckglaser cover glass (Fisher Scientific cat#NC1776158).  
199 All incubations and washes were done at room temperature with gentle rocking. Human tissue was  
200 immunolabeled identically to mice with the exception that the step incubating sections in vehicle  
201 containing 0.1 mg/mL IgG F(ab) polyclonal IgG antibody was omitted and sections were incubated in  
202 primary antibodies for 2 hours instead of 1. Primary antibodies used in Figure 2 and Figure 3 were used  
203 at saturating concentrations (Supplemental Figure 4).

204

### 205 ***Imaging***

206 Images were acquired with an inverted scanning confocal and airy disk imaging system (Zeiss LSM 880  
207 Airyscan, 410900-247-075) run by ZEN black v2.1. Laser lines were 405 nm, 488 nm, 543 nm and 633 nm.  
208 Low-magnification images to image whole mouse DRG were acquired in confocal or airy disk imaging  
209 mode with a 0.8 NA 20x objective (Zeiss 420650-9901) details in figure legends. Images containing both  
210 the DRG and spinal cord were tile scan images acquired in confocal mode with the same 20x objective.  
211 When imaging whole DRG for Figure 2 and Figure 3 the imaging plane was selected using fluorescence  
212 from channels that did not contain anti-Kv2.1 or anti-Kv2.2 immunofluorescence. High-magnification  
213 images were acquired in airy disk imaging mode with a 1.4 NA 63x oil objective (Zeiss 420782-9900-799).  
214 Linear adjustments to contrast and brightness and average fluorescence intensity z-projections were  
215 performed using ImageJ software.

216

### 217 ***Image Analysis***

218 Images were analyzed using ImageJ software (Schindelin et al., 2012). A summary of automated analysis  
219 for selecting neurons in DRG sections can be found in Supplemental Figure 5. The ImageJ plugin  
220 MorphoLibJ was used for performing watershed segmentation of images (Legland, Arganda-Carreras, &  
221 Andrey, 2016). Automatic generation of ROIs from watershed segmentation did not distinguish the  
222 presence of nuclei and is thus expected to over-count larger diameter neurons. Unless stated otherwise  
223 the region of DRG neurons used to analyze anti-Kv2 immunofluorescence is the outer edge  
224 (Supplemental Figure 5 I). Immunofluorescence is defined as the raw pixel values from confocal images  
225 and was not background subtracted. We noted that in smaller neurons the nucleus takes up a greater  
226 percentage of the total volume and could skew fluorescence measurements if fluorescence in the entire  
227 soma volume is measured. As Kv2 protein is not present in the nucleus and is enriched at the outer edge  
228 (Figure 1) we found that measuring anti-Kv2 immunofluorescence at the outer edge of the neuron  
229 reduces potential error that could be associated with soma diameter. For proteins that were not Kv2

230 channels we analyzed the immunofluorescence of the entire soma as these proteins did not exhibit the  
231 same enrichment at the outer edge as Kv2 channels (Figure 9 B). Where specified, manual ROIs were  
232 used in analysis otherwise automatically generated ROIs were used. When analyzing  
233 immunofluorescence from human neurons, ROIs were drawn around areas within the neuronal soma  
234 that do not contain apparent lipofuscin (Supplemental Figure 11 C). Fitting of imaging data was  
235 performed using Igor Pro software version 8 (Wavemetrics, Lake Oswego, OR) that employs nonlinear  
236 least square curve fitting via the Levenberg-Marquardt algorithm. Distributions of fluorescence intensity  
237 from DRG neurons were fit with a log normal distribution:

238

$$239 \quad f(x) = A \exp\left[-\frac{\left[\ln\left(\frac{x}{x_0}\right)\right]^2}{width}\right] \quad (\text{Equation 1})$$

240

241 Where A = amplitude,  $x_0$  = mean, and width =  $\sqrt{2}$  times standard deviation. Concentration-effect  
242 experiments in Supplemental Figure 4 were fit with the Hill equation:

243

$$244 \quad f(x) = base + \frac{max-base}{1 + \left(\frac{x_{half}}{x}\right)^n} \quad (\text{Equation 2})$$

245

#### 246 **Code Accessibility**

247 In-house Fiji macros and R script used to process imaging data are available for download at  
248 <https://github.com/SackLab/DRG-Image-Processing>

249

#### 250 **Statistics**

251 All statistical tests were performed in Igor Pro software version 8 (Wavemetrics, Lake Oswego, OR).

252 Independent replicates (n) are individual neurons while biological replicates (N) are individual mice. The

- 253 n and N values for each figure are listed in Table 1. Details of statistical tests are in the figure legends.
- 254 We did not observe a difference between males and females in detectable Kv2.1 or Kv2.2 protein, but
- 255 animal numbers were not sufficient for rigorous statistical comparison.

256 **RESULTS**

257

258 **Kv2.1 and Kv2.2 immunolabeling is enriched at the apparent plasma membrane of DRG neuron**

259 **somata**

260

261 To assess the cellular expression and subcellular localization of Kv2.1 and Kv2.2 voltage gated potassium  
262 channels in DRG neurons we used a set of anti-Kv2.1 and anti-Kv2.2 antibodies that have previously  
263 been validated in brain tissue from Kv2 knockout mice (Bishop et al., 2015) to perform multiplex  
264 immunofluorescence labeling of DRG neurons. Anti-Kv2.1 (magenta) and anti-Kv2.2 (green)  
265 immunofluorescence is prominent in DRG neuron somata (Figure 1 A). In neurons we observed anti-  
266 Kv2.1 and anti-Kv2.2 immunofluorescence enriched at the outer edge of DRG neuron somata consistent  
267 with their plasma membrane localization (Figure 1 B arrows). This putative cell surface localization is  
268 distinct from prior reports of anti-Kv2 immunofluorescence in DRG (Tsantoulas et al., 2012) as well as  
269 that for other ion channel proteins such as Nav1.8 (Shields et al., 2012) and TRPV1 (Cho & Valtschanoff,  
270 2008), all of which are primarily in the cytoplasm. Anti-Kv2.1 or anti-Kv2.2 immunofluorescence at the  
271 edge of neuron somata was more apparent when imaging thinner optical sections. To determine if  
272 enrichment of Kv2 immunolabeling at the outer edge of DRG neurons was an artifact of our  
273 immunohistochemistry or imaging protocols, we additionally labeled DRG sections with a knockout-  
274 validated antibody against Nav1.8. In the same DRG section labeled for Kv2 channels, cytoplasmic anti-  
275 Nav1.8 immunofluorescence was prominent in small to medium diameter lumbar DRG neurons,  
276 consistent with previous reports (He et al., 2010; Shields et al., 2012) (Figure 1 B). To quantify  
277 enrichment of anti-Kv2 versus anti-Nav1.8 immunofluorescence at the outer edge of DRG neurons, we  
278 manually drew regions of interest (ROIs) for each DRG soma. We generated a 2  $\mu\text{m}$  wide annulus that  
279 encompassed the outer edge and a second 2  $\mu\text{m}$  wide annulus just inside the first one (Figure 1 C arrows

280 1 and 2 respectively). By comparing the fluorescence intensity of immunofluorescence signals within  
281 these annuli we found that the edge of DRG neuron somata is enriched for anti-Kv2.1 and anti-Kv2.2  
282 immunofluorescence relative to that of Nav1.8 (ANOVA  $< 0.001$ ) (Figure 1 D). Similarly, anti-Kv2.1 and  
283 anti-Kv2.2 immunofluorescence is enriched at the edge of DRG neuron somata relative to anti-TRPV1  
284 immunofluorescence (ANOVA  $< 0.001$ ) (Supplemental Figure 3).

285

### 286 **The majority of dorsal root ganglion neurons express Kv2 protein**

287

288 To determine whether the anti-Kv2.1 immunofluorescence signal in DRG sections is specific and  
289 dependent on the presence of Kv2.1 protein, we compared fluorescence intensities in DRG samples  
290 prepared in parallel from age and sex matched wild-type (WT) mice and Kv2.1 knock-out (KO) mice. We  
291 observed anti-Kv2.1 immunolabeling in WT DRG neurons that was absent from Kv2.1 KO, while  
292 fluorescence corresponding to an antibody that targets  $\beta$ III tubulin was similar in both WT and Kv2.1 KO  
293 mice (Figure 2 A). To quantify fluorescence intensities of DRG sections, we manually drew ROIs around  
294 neuron soma profiles with clearly visible nuclei and measured the fluorescence intensity at the outer  
295 edge of profiles as shown in Figure 1 C. We define a profile as a slice of a DRG neuron in a histological  
296 section (Coggeshall, 1992). We found that 99% of manually identified profiles from the WT mouse DRG  
297 shown in Figure 2 A had anti-Kv2.1 immunofluorescence above the mean of Kv2.1 KO mice (Figure 2 B).  
298 To reduce human bias in identification of profiles we used an automated method to generate ROIs. As  
299 with the manual method, the automated method reliably identified neuronal profiles (Supplemental  
300 Figure 5 I). However, the automated method did not distinguish profiles without nuclei which could lead  
301 to overrepresentation of larger neurons (Coggeshall, 1992; Coggeshall & Lekan, 1996). Additionally, the  
302 automated method occasionally selected ROIs which did not appear to be neurons (Supplemental Figure  
303 5 H red arrows). Despite these limitations, the absolute reproducibility of the automated method when

304 scaled to identify thousands of neuronal profiles indicated that automated ROIs could provide a rigorous  
305 means of identifying neuronal profiles for statistical analysis. In automatically generated ROIs from the  
306 same WT mouse manually analyzed in Figure 2 B we observed a reduction in the mean anti-Kv2.1 but  
307 not anti- $\beta$ III immunofluorescence in Kv2.1 KO mice (Figure 2 C and D). We found that 89% of  
308 automatically generated ROIs had anti-Kv2.1 immunofluorescence above the mean of the paired Kv2.1  
309 KO mouse. We manually identified that 9% of the automatically generated ROIs from the WT mouse did  
310 not appear to be neurons, suggesting that 98% of profiles in this automated dataset could have anti-  
311 Kv2.1 immunofluorescence above the mean of the Kv2.1 KO mouse, consistent with manual analysis.  
312 We expanded the automated method to 5 pairs of age and sex matched WT and Kv2.1 KO mice, and  
313 found that anti-Kv2.1 immunofluorescence was significantly reduced in each matched Kv2.1 KO mouse  
314 relative to anti-Kv2.2 or anti- $\beta$ III tubulin immunofluorescence while no significant difference was  
315 observed between anti-Kv2.2 and anti- $\beta$ III tubulin (Figure 2 E) (ANOVA  $p < 0.001$ ). We identified that  $93$   
316  $\pm 6\%$  (SD) of ROIs from the five WT mice had anti-Kv2.1 immunofluorescence above the mean of age and  
317 sex matched Kv2.1 KO mice (Figure 2 F). This analysis confirms that anti-Kv2.1 immunofluorescence  
318 reveals Kv2.1 protein at neuron surfaces.

319

320 We developed a method to estimate the fraction of ROIs that contain detectable Kv2.1 protein. The  
321 histogram of fluorescence intensity in automatically generated ROIs from Kv2.1 KO DRG sections labeled  
322 with an anti-Kv2.1 antibody had variability which could reasonably be fit with a log normal distribution  
323 (equation 1) (Figure 2 G). We assumed a similar distribution of background immunofluorescence is also  
324 present in neuron profiles of age and sex matched WT mice and fit the Kv2.1 KO distribution to the WT  
325 histogram to estimate the fraction of ROIs without detectable Kv2.1 (Figure 2 H red gaussian). Using this  
326 method, we compared Kv2.1 immunofluorescence in DRG sections of multiple age and sex matched WT  
327 and Kv2.1 KO mice. The fitting indicated that  $84 \pm 9\%$  (SD) of automatically generated ROIs from WT

328 mice have detectable Kv2.1 protein (N = 5 pairs of mice) (Figure 2 I). As approximately 9% of ROIs are  
329 expected to not contain neurons these results suggest that greater than 90% of mouse DRG neurons  
330 have detectable Kv2.1 protein. We further validated our automated methodology with a transgenic  
331 MrgprD-GFP mouse line that expresses GFP in non-peptidergic nociceptors that comprise approximately  
332 19-24% of all lumbar DRG neurons (Dirajlal, Pauers, & Stucky, 2003; Dong, Han, Zylka, Simon, &  
333 Anderson, 2001; Wang & Zylka, 2009). In comparing the MrgprD-GFP mice to WT C57BL/6J mice we  
334 found that  $23 \pm 15\%$  (SD) of automatically generated profiles (N = 4 pairs of mice) had detectable GFP  
335 (Supplemental Figure 6).

336  
337 We compared anti-Kv2.2 immunofluorescence from an age and sex matched WT and Kv2.2 KO mouse by  
338 drawing ROIs around neuron soma profiles with clearly visible nuclei. This identified that greater than  
339 99% of WT profiles have anti-Kv2.2 immunofluorescence above the mean immunofluorescence of the  
340 paired Kv2.2 KO mouse (Figure 3 B). Automatically generated ROIs for multiple age and sex matched WT  
341 and Kv2.2 KO mice indicate that  $91 \pm 5\%$  (SD) of ROIs from WT mice have detectable Kv2.2 protein (N = 8  
342 pairs of mice) (Figure 3 F-H). Using the automated analysis, we found that anti-Kv2.2  
343 immunofluorescence was significantly reduced in Kv2.2 KO mice relative to anti-Kv2.1 or anti-NF200  
344 immunofluorescence in age and sex matched WT and Kv2.2 KO mice (ANOVA  $p < 0.001$ ) while no  
345 significant difference between anti-NF200 or anti-Kv2.1 immunofluorescence was observed (Figure 3 A-  
346 E). These combined results suggest that more than 90% of neuron profiles contain detectable Kv2.1 or  
347 Kv2.2 protein, raising the possibility that all mouse DRG neurons express Kv2 channels.

348

349 **Kv2.1 immunolabeling decreases in older mice while Kv2.2 immunolabeling remains similar**

350

351 Kv2.2 transcript in mouse DRG decreases during postnatal development (Regnier et al., 2016) and Kv2.1  
352 protein expression in mouse brain decreases with age (Cotella et al., 2012; Regnier et al., 2016). To  
353 identify if Kv2 protein levels in DRG neurons vary between young adult and old mice we compared anti-  
354 Kv2.1 and anti-Kv2.2 immunofluorescence from samples subjected to identical immunolabeling and  
355 imaging protocols. We observed lower anti-Kv2.1 (Figure 4 A, B and C) in DRG sections from 50 week old  
356 mice relative to 7-16 week old mice. Comparisons with Kv2.1 KO mice indicate that  $50 \pm 23\%$  (SD) of  
357 ROIs from 50 week old mice express detectable Kv2.1 protein, significantly less ( $p = 0.018$ ) than the  $84 \pm$   
358  $9\%$  (SD) of ROIs with detectable Kv2.1 protein from 7-16 week old mice (Figure 4 D). In contrast, similar  
359 anti-Kv2.2 immunofluorescence was seen in samples from young adult and old mice (Figure 4 E, F and  
360 G). Comparisons with Kv2.2 KO mice indicate that  $96 \pm 3\%$  of profiles from 50 week old mice express  
361 detectable Kv2.2 protein, a weakly significant increase ( $p = 0.03$ ) from the  $88 \pm 3\%$  (SD) of profiles with  
362 detectable Kv2.2 protein from 7-24 week old mice (Figure 4 H). We note that this weak statistical  
363 increase is underpowered due to the availability of only three 50 week old Kv2.2 KO mice.

364

365 **Kv2 channels are expressed on the cell surface of acutely dissociated DRG neurons**

366

367 To determine if Kv2 channels are present on neuron surfaces we labeled live acutely dissociated DRG  
368 neurons with a cell-impermeant fluorescent probe which binds Kv2 channels. The probe is a variant of  
369 the tarantula peptide guangxitoxin-1E conjugated to Alex Fluor 594 (GxTX-594) which binds to an  
370 extracellular site of Kv2.1 and Kv2.2 channels (Thapa et al., 2021). We applied GxTX-594 to live  
371 dissociated DRG neurons from WT mice and double knockout (DKO) mice lacking expression of both  
372 Kv2.1 and Kv2.2 protein (Figure 5). In WT DRG neurons, we observed fluorescence at the membrane

373 after application of 100 nM GxTX-594 that was not present before the addition of GxTX-594 (Figure 5 A).  
374 Wheat germ agglutinin conjugated to Alexa 405 (WGA-405) was used to identify the surface membrane  
375 of cultured DRG neurons and confirmed that the GxTX-594 fluorescence observed in WT neurons was  
376 cell surface localized (Figure 5 A middle). The cell surface localized fluorescence of GxTX-594 observed in  
377 WT neurons was not present in Kv2.1/Kv2.2 DKO neurons (Figure 5 B). To quantify the cell surface-  
378 associated fluorescence signals of individual WT and Kv2.1/Kv2.2 DKO neurons, we used an automated  
379 method to generate ROIs corresponding to the WGA-405 fluorescence and measured GxTX-594 labeling  
380 within this ROI (Figure 5 C). This analysis confirmed a reduction in GxTX-594 fluorescence at the  
381 membrane in cultured DRG neurons from Kv2.1/Kv2.2 DKO mice compared to WT mice (Figure 5 D).  
382 Similar to the Kv2 immunofluorescence signals from KO mice (Figures 2 and 3), GxTX-594 fluorescence  
383 from Kv2.1 /Kv2.2 DKO mice could be reasonably fit with a log normal distribution (equation 1) (Figure 5  
384 E). Applying the same method used to estimate the fraction of neuronal profiles expressing detectable  
385 Kv2.1 and Kv2.2 immunofluorescence we compared cultured DRG neurons of age and sex matched WT  
386 and Kv2.1/Kv2.2 DKO mice and estimated that  $76 \pm 2.4\%$  (SD) of DRG neurons have detectable cell  
387 surface GxTX-594 fluorescence (Figure 5 F and G). This indicates that at least 76% of neurons express  
388 Kv2 channels in their surface membrane, consistent with a report of Kv2 conductance in every DRG  
389 neuron type assessed (Zheng et al., 2019) .

390

### 391 **Anti-Kv2.2 immunofluorescence is enriched in DRG neurons relative to spinal cord neurons**

392

393 In mammals, anti-Kv2.1 and anti-Kv2.2 immunofluorescence is apparent in central neurons of the brain  
394 (Kihira et al., 2010; Bishop et al., 2015) and anti-Kv2.1 in the spinal cord (Bishop et al., 2015; Muennich &  
395 Fyffe, 2004). We measured Kv2 immunofluorescence intensities in sections of mouse spinal column  
396 which contain both the DRG and the spinal cord. Neurons in the ventral and dorsal horn of the spinal

397 cord exhibit anti-Kv2.1 immunofluorescence (Figure 6 A). We observed anti-Kv2.1 puncta on neurons in  
398 the ventral horn (Figure 6 A inset) similar to that described in alpha motor neurons (Fletcher et al., 2017;  
399 Romer et al., 2014). Fewer spinal cord neurons exhibit anti-Kv2.2 immunofluorescence than anti-Kv2.1  
400 (Figure 6 A and Supplemental Figure 7 A arrow heads). Kv2.2 channel protein in the spinal cord of mice  
401 has to our knowledge not been assessed, but anti-Kv2.2 immunofluorescence has been observed early  
402 in development in the ventrolateral spinal cord in the frog *Xenopus laevis* (Gravagna, Knoeckel, Taylor,  
403 Hultgren, & Ribera, 2008). We analyzed anti-Kv2 immunofluorescence from individual neurons in the  
404 DRG and ventral horn of five mice and found that while anti-Kv2.1 immunofluorescence is similar  
405 between the two regions (Figure 6 B), anti-Kv2.2 immunofluorescence is significantly higher in DRG  
406 neurons relative to ventral horn neurons (Figure 6 C). Approximately 30% of neurons in the DRG have  
407 anti-Kv2.2 immunofluorescence at a level higher than the brightest anti-Kv2.2 immunofluorescence  
408 observed in the spinal cord. We repeated this analysis with a different anti-Kv2.2 antibody and found  
409 similar results (Supplemental Figure 7).

410

411 **Kv2 channels on DRG neuron somata and stem axons form clustered subcellular patterns with**  
412 **similarities to and distinctions from central neurons.**

413

414 In neurons throughout the brain (Trimmer, 1991, Scannevin et al., 1996, Bishop et al., 2015) and motor  
415 neurons in the spinal cord (Muennich and Fyffe, 2004), Kv2 channels form punctate structures referred  
416 to as clusters. In central neurons, Kv2 clusters localize to the soma, proximal dendrites and axon initial  
417 segment (Lim, Antonucci, Scannevin, & Trimmer, 2000; Scannevin et al., 1996; Trimmer, 1991). At  
418 clusters, Kv2 channels organize protein signaling complexes and endoplasmic reticulum-plasma  
419 membrane junctions (Johnson et al., 2018; Kirmiz et al., 2018; Panzera et al., 2022; Vierra et al., 2021).  
420 To determine whether Kv2 channels in DRG neurons form clusters similar to central neurons, we

421 compared *en face* z-projections of Kv2 clusters in DRG neurons and ventral horn neurons in the same  
422 spinal cord section (Figure 7). Anti-Kv2.1 immunofluorescence in the ventral horn neurons of these mice  
423 resembles previous reports of mice (Fletcher et al., 2017) and rats (Fletcher et al., 2017; Muennich &  
424 Fyffe, 2004). In both DRG and spinal cord neurons, Kv2.1 and Kv2.2 channels form dense clusters (Figure  
425 7 A and B). Kv2 channel clusters in DRG typically appeared smaller than Kv2 clusters in spinal cord.  
426 However, we are not certain these observations in fixed tissue represent the *in vivo* arrangement, as  
427 Kv2.1 channels in brain neurons can decluster in the period between sacrifice and fixation (Misonou et  
428 al., 2005). In some DRG neurons, we observed donut shaped Kv2.1 and Kv2.2 clusters (Figure 7 B and C  
429 insets) which resemble donut shaped Kv2 clusters in interneurons which harbor specialized protein  
430 machinery in their center (Vullhorst et al., 2015).

431  
432 DRG neurons are distinct from central neurons as they have a single stem axon that exits the cell soma  
433 and bifurcates into the central and peripheral axon branches (Ha, 1970). We observed punctate  
434 immunofluorescence for both Kv2.1 and Kv2.2 on the apparent stem axons of DRG neurons (Figure 7 B,  
435 D and E arrow heads, Supplemental Figure 8). In DRG sections from the *MrgprD<sup>GFP</sup>* mouse line we  
436 observed Kv2 clusters on the stem axon of GFP-expressing neurons. As *MrgprD<sup>GFP</sup>* marks non-peptidergic  
437 nociceptors (Zheng et al., 2019) we confirm stem axon localization in this subpopulation of  
438 unmyelinated neurons (Supplemental Figure 8 A).

439  
440 While Kv2 clusters in central neurons and many DRG neurons are distributed evenly throughout the  
441 soma, we found that DRG neurons asymmetrically distribute Kv2 clusters on the soma (Figure 7 B-E  
442 arrows). To test if enrichment of Kv2 channel clusters is oriented to a specific region on the soma we  
443 manually traced the surface of neurons whose apparent stem axons were visible (Figure 7 F). The  
444 brightest anti-Kv2.1 and anti-Kv2.2 immunofluorescence is near the stem axon in 76 and 80% of DRG

445 neurons respectively (Figure 7 G and H). Asymmetric distribution of Kv2 channels is not frequently  
446 observed in central neurons of mice (Bishop et al., 2018; Bishop et al., 2015; Romer et al., 2014)  
447 suggesting a potentially unique role of Kv2 subcellular organization in DRG neurons.

448

#### 449 **Kv2.2 channels are expressed in peripheral axons of DRG neurons**

450

451 To determine if anti-Kv2 immunofluorescence is detectable in DRG axons in regions beyond the stem  
452 axon we immunolabeled samples containing both peripheral and central axons, using NF200 or  $\beta$ III  
453 tubulin as markers for DRG axons which target myelinated neurons or all DRG neurons respectively.  
454 Neurons were not co-labeled with  $\beta$ III tubulin and Kv2.2 targeting antibodies because they were of the  
455 same isotype. We did not observe anti-Kv2.1 immunofluorescence in peripheral axons (Supplemental  
456 Figure 9) from the same DRG section that had detectable anti-Kv2.1 immunofluorescence in neuron  
457 somas (Figure 2). However, anti-Kv2.2 immunofluorescence is detectable in peripheral and central axons  
458 of WT but not Kv2.2 KO mice (Figure 8 B and C). Anti-Kv2.2 immunofluorescence on myelinated  
459 peripheral axons appears as discrete puncta or as larger bands which span the width of the axon (Figure  
460 8 B arrows). We also observed anti-Kv2.2 immunofluorescence not colocalized with NF200, suggestive of  
461 unmyelinated fibers (Figure 8 B arrow head). In *MrgprD<sup>GFP</sup>* mice, anti-Kv2.2 immunofluorescence  
462 colocalizes with axons expressing cytosolic GFP, identifying that non-peptidergic nociceptors also  
463 express Kv2.2 protein along the peripheral axon (Figure 8 D). We further investigated the expression of  
464 Kv2.2 in peripheral myelinated fibers by co-labeling peripheral axons with antibodies specific for CASPR  
465 (Einheber et al., 1997) and Kv1.2 (Rasband et al., 1998) which identify the paranodal and juxtaparanodal  
466 regions of nodes of Ranvier, respectively in myelinated fibers. We found punctate anti-Kv2.2  
467 immunofluorescence associated with both CASPR and Kv1.2 in some WT DRG neuron axons that is not  
468 present in Kv2.2 KO mice (Supplemental Figure 10 A). We analyzed anti-Kv2.2 immunofluorescence in

469 WT and Kv2.2 KO mice by manually drawing ROIs around CASPR and Kv1.2 immunofluorescence while  
470 blinded to anti-Kv2.2 immunofluorescence and found that 26/34 CASPR and 20/31 Kv1.2  
471 immunolabeled regions had anti-Kv2.2 immunofluorescence brighter than the brightest anti-Kv2.2  
472 immunofluorescence measured in Kv2.2 KO mice (Supplemental Figure 10 B). These results indicate that  
473 Kv2.2 but not Kv2.1 protein is detectable in axons of myelinated and unmyelinated somatosensory  
474 neurons. However, these results do not identify if Kv2.2 channels are localized to specific subcellular  
475 regions of somatosensory axons.

476

#### 477 **Anti-Kv2.1 and anti-Kv2.2 immunofluorescence is non-uniform across DRG neuron subtypes**

478

479 Different voltage gated potassium channels make distinct contributions to outward potassium currents  
480 in sensory neuron subtypes (Zheng et al., 2019). We observed subpopulations of DRG neurons that have  
481 bright anti-Kv2.1 immunofluorescence but dim anti-Kv2.2 immunofluorescence and vice-versa (Figure 9  
482 A and C, Figure 1 A, and Figure 6 A). We hypothesized that differences in Kv2.1 and Kv2.2 protein density  
483 could potentially denote specific subtypes of sensory neurons. In order to test if relative density of Kv2.1  
484 and Kv2.2 protein differs in subtypes of DRG neurons, we assessed anti-Kv2.1 and anti-Kv2.2  
485 immunofluorescence in four DRG neuron subtypes. Neurons identified by genetically encoded markers  
486 were GFP-expressing neurons from *MrgprD<sup>GFP</sup>* mice which we refer to as non-peptidergic nociceptors  
487 (Zheng et al., 2019), or tdTomato-expressing neurons from *PV<sup>Ai14</sup>* mice which we refer to as  
488 proprioceptors (Zheng et al., 2019). Neurons immunolabeled for CGRP we refer to as peptidergic  
489 nociceptors (Zheng et al., 2019) and neurons immunolabeled for NF200 we refer to as myelinated DRG  
490 neurons (Usoskin et al., 2015) (Figure 9 B and D). We quantified detectable Kv2.1 or Kv2.2 protein  
491 density in individual ROIs by rank ordering the immunofluorescence intensity. Rank orders from multiple  
492 mice were pooled with a value of 100% representing the brightest ROI in each mouse (Figure 9 D). The

493 rank percentiles of Kv2.1 and Kv2.2 have similar distributions in peptidergic and non-peptidergic  
494 nociceptors. Many ROIs with the highest Kv2.1 or Kv2.2 rank percentile were NF200-positive myelinated  
495 neurons. Proprioceptors, a subset of the myelinated neurons, appear to account for the subpopulation  
496 of neurons with bright anti-Kv2.2 and dim anti-Kv2.1, and have high rank percentiles of Kv2.2 but low  
497 rank percentiles of Kv2.1. (Figure 9 A, B, and C). Profiles with bright anti-Kv2.1 and dim anti-Kv2.2  
498 immunofluorescence are mostly NF200-positive myelinated neurons of unknown subtype (Figure 9 A, B,  
499 and C blue points). Overall, these results identify that the relative densities of Kv2.1 and Kv2.2 protein  
500 are similar in DRG neuron subtypes except proprioceptors. These results are consistent with reports that  
501 Kv2.1 and Kv2.2 mRNA transcript levels are similar in DRG neuron subtypes except proprioceptors. Our  
502 finding that Kv2.1 protein density is anomalously low in proprioceptors mirrors the finding that Kv2.1  
503 transcripts are also low in proprioceptors (Usoskin et al., 2015; Zheng et al., 2019).

504

#### 505 **Kv2 channel cellular expression and subcellular localization in human DRG neurons is similar to mice**

506

507 Kv2 mRNA transcripts are present in human DRG neurons (Tavares-Ferreira et al., 2022; Wangzhou et  
508 al., 2020), and we assessed whether anti-Kv2 immunofluorescence is associated with human DRG  
509 neurons. As human Kv2.1 and Kv2.2 knockout controls are not available, we compared fluorescence in  
510 DRG sections with anti-Kv2 primary antibodies to those lacking primary antibodies. Control samples  
511 lacking primary antibodies revealed strong autofluorescence at all excitation wavelengths (Supplemental  
512 Figure 11 A and B) consistent with other studies of human DRG neurons which have attributed this  
513 autofluorescence to lipofuscin (Shiers et al., 2021). We found that most neurons have anti-Kv2.1 and  
514 anti-Kv2.2 immunofluorescence brighter than controls lacking primary antibodies (Supplemental Figure  
515 11 D and E) suggesting that Kv2 protein is present in human DRG neurons. As a control, we used the  
516 same methods with anti-Nav1.7 and anti-Nav1.8 antibodies and found anti-Nav1.7 immunofluorescence

517 in nearly all human DRG neurons while anti-Nav1.8 was in a smaller fraction of DRG neurons, consistent  
518 with previous reports of Nav1.7 protein and Nav1.8 transcript in human DRG (Shiers, Klein, & Price,  
519 2020) (Supplemental Figure 11 A arrow heads, B, F and G). Similar to DRG neurons in mice, we observed  
520 subpopulations of neurons that had bright anti-Kv2.1 immunofluorescence but dim anti-Kv2.2  
521 immunofluorescence and conversely neurons that had bright anti-Kv2.2 immunofluorescence but dim  
522 anti-Kv2.1 immunofluorescence (Figure 10 A and B). These observations were consistent in DRG from 3  
523 human donors (Supplemental Figure 11 A and H and Supplemental Figure 12). We were unable to  
524 identify if the population of human DRG neurons with low anti-Kv2.1 and high anti-Kv2.2 are  
525 proprioceptors as we observed in mice; attempts to label parvalbumin in human neurons were  
526 unsuccessful.

527  
528 We assessed whether Kv2 protein subcellular localization in humans is similar to mice. We identified  
529 neurons in all three human DRG samples where anti-Kv2.1 and anti-Kv2.2 immunofluorescence was  
530 enriched at the outer edge of DRG neuron somata (Figure 10 A arrow and Supplemental Figure 13). In  
531 some neurons from all three humans, Kv2 clusters exhibited asymmetric distribution on the neuronal  
532 soma (Figure 10 B green arrow head, Supplemental Figure 13 A-E arrows). In one human we identified a  
533 neuron with Kv2.2 immunofluorescence that was asymmetrically distributed near the stem axon  
534 consistent with observations in mice (Figure 10 B green arrow). We identified Kv2.2  
535 immunofluorescence on the stem axon of DRG neurons in all three humans using anti-NF200 or anti-  
536 Nav1.7 as markers of the stem axon (Figure 10 B-C and Supplemental Figure 14 arrows). In two out of  
537 three humans we also identified Kv2.1 immunofluorescence on the stem axon of human DRG neurons  
538 (Figure 10 C inset and Supplemental Figure 14 B and D inset). To determine if Kv2.2 channels are present  
539 in human DRG neuron axons, we labeled human DRG sections with the same anti-Kv2.2, anti-NF200,  
540 anti-CASPR and anti-Kv1.2 antibodies that were used in mice. We found anti-Kv2.2 immunofluorescence

541 associated with anti-NF200, anti-CASPR and anti-Kv1.2 immunofluorescence in human DRG neuron  
542 axons (Supplemental Figure 15) suggesting that Kv2.2 channels could contribute to electrical  
543 propagation or other physiological functions in axons of human DRG neurons.

544

## 545 **DISCUSSION**

546

547 Our results reveal overlapping yet distinct localization patterns of Kv2.1 and Kv2.2 in DRG neurons. Here,  
548 we discuss the unique features of Kv2 localization in the DRG and how these could influence neuronal  
549 physiology and somatosensation.

550

551 We identify differences between anti-Kv2.1 and anti-Kv2.2 immunofluorescence in DRG neurons. Kv2.2  
552 mRNA is abundant in all DRG neuron subtypes identified, while Kv2.1 mRNA is low in proprioceptors and  
553 abundant in other subtypes (Usoskin et al., 2015; Zheng et al., 2019). Consistent with these findings we  
554 conservatively estimate that Kv2.1 and Kv2.2 protein is in at least 90% of mouse DRG neurons, though  
555 Kv2.1 immunofluorescence is anomalously low in proprioceptors. Detection of Kv2.2 but not Kv2.1 in  
556 DRG neuron peripheral and central axons suggests that Kv2.2 channels may be important for electrical  
557 transmission in these axons. While detectable Kv2.2 remained constant in DRG neurons of older mice,  
558 detectable Kv2.1 decreased, possibly contributing to the altered repolarization noted in DRG neurons  
559 from aged mice (Scott, Leu, & Cinader, 1988). The differences between Kv2.1 and Kv2.2 in  
560 somatosensory neurons are consistent with distinct roles for these Kv2 paralogs in somatosensory  
561 neuron physiology, as seen in brain and pancreatic islets (Bishop et al., 2015; Johnston et al., 2008; Li et  
562 al., 2013).

563

564 The expression and subcellular localization of Kv2 channels in DRG neurons are distinct from central  
565 neurons. Kv2.1 is present in most brain neurons (Bishop et al., 2018; Bishop et al., 2015; Hwang, Fotuhi,  
566 Bredt, Cunningham, & Snyder, 1993) while Kv2.2 is less broadly expressed (Bishop et al., 2015;  
567 Hermanstynne et al., 2010; Hwang, Glatt, Bredt, Yellen, & Snyder, 1992; Johnston et al., 2008; Kihira et  
568 al., 2010). In contrast to this, we find Kv2.2 expressed in at least 90% of mouse DRG neurons. We also  
569 identify that Kv2.2 is enriched in the DRG relative to neurons in the spinal cord, suggesting that  
570 abundant Kv2.2 protein expression is a distinct feature of DRG neuron physiology. In central neurons,  
571 Kv2 channel clusters are typically evenly distributed across neuron somata (Bishop et al., 2015; Kihira et  
572 al., 2010; Muennich & Fyffe, 2004) and asymmetric subcellular localization of Kv2 clusters on neuron  
573 somata has to our knowledge not been described. We find that Kv2 channels are enriched at the plasma  
574 membrane in a subcellular region near the stem axon of some DRG neurons. Differences in Kv2  
575 localization between central and somatosensory neurons could arise from differences in the  
576 extracellular environment surrounding DRG neuron somata. In central neurons, Kv2 channel clusters are  
577 reported at cholinergic C-terminal synaptic sites, S-type synapses, and apposed to astrocytic end feet  
578 (Du et al., 1998; Muennich & Fyffe, 2004). However, synapses have not been reported in the DRG and  
579 DRG neurons are surrounded by satellite glia instead of astrocytes (Matsuda et al., 2005). Further  
580 studies could investigate if Kv2 clusters are localized to extracellular structures in the DRG. Kv2.2 has  
581 been identified in juxtaparanodes but not paranodes of axons in the osseous spiral lamina of the cochlea  
582 (Kim & Rutherford, 2016) and previous work has also identified that Kv2.1 channels are necessary for  
583 enabling ER Ca<sup>2+</sup> uptake during electrical activity in both the soma and axon (Panzera et al., 2022). To  
584 our knowledge, Kv2.2 immunofluorescence has not been previously reported in distal axons in the brain,  
585 spinal cord or DRG. Our results indicate that Kv2.2 channels are present in myelinated and unmyelinated  
586 axons of DRG neurons. The mechanism of Kv2.2 protein trafficking to the axon is unknown. Kv2.1  
587 channels are trafficked to the axon initial segment through a distinct secretory pathway (Jensen et al.,

588 2017) allowing neurons to regulate precise compartment specific localization of Kv2.1 protein. A similar  
589 mechanism for Kv2.2 localization in DRG axons could allow neurons to independently control Kv2.2  
590 protein expression in the neuron soma and axon. The subcellular distribution of Kv2.1 and Kv2.2  
591 subunits in DRG neurons suggests they could each distinctly modulate electrical signals. We note that  
592 our observations could not distinguish whether immunofluorescence in DRG axons could represent  
593 intracellular trafficking vesicles of Kv2.2 proteins, or whether axonal Kv2.2 is on the membrane surface  
594 where it could modulate electrical signals.

595

596 Kv2 channels in DRG neurons may play important roles in somatosensation and nociception. Kv2  
597 conductances can modulate action potential repolarization, afterhyperpolarization and repetitive firing  
598 (Liu & Bean, 2014; Zheng et al., 2019). Kv2 conductances modulate electrical transmission in rat DRG  
599 neurons (Tsantoulas et al., 2014). Knockdown of Kv2.1 increases hypersensitivity to painful stimuli and  
600 regulation of Kv2.1 protein expression through the epigenetic factor Cdy1 modulates neuronal  
601 excitability and nociception (Sun et al., 2022). Consistent with these studies, our results show that Kv2  
602 channels are localized to DRG neuron axons, where they could potentially influence electrical  
603 transmission.

604

605 Regulatory pore-forming subunits of the Kv5, Kv6, Kv8, and Kv9 "silent subunit" families obligately  
606 assemble into heteromeric channels with Kv2 subunits (Bocksteins, 2016) and have been implicated in  
607 nociception. Women with decreased sensitivity to labor pain were identified to have a mutation in the  
608 Kv6.4 silent subunit that disrupts Kv2.1/Kv6.4 heteromer expression and is proposed to modulate  
609 nociceptor signaling (Lee et al., 2020). Downregulation of the Kv9.1 silent subunit after axotomy evokes  
610 hyperexcitability of DRG neurons (Tsantoulas et al., 2012). While both Kv2 channels are broadly  
611 expressed in DRG neurons, transcript levels of silent subunits in mice and humans show much more

612 neuron subtype specificity (Tavares-Ferreira et al., 2022; Zheng et al., 2019), raising the possibility of  
613 molecularly distinct Kv2-containing channels in somatosensory neuron subtypes.

614

615 Previous studies have identified that voltage gated ion channel expression can be substantially different  
616 between mice and human DRG, notably, in the expression of Nav1.7 (Shiers et al., 2020). However, we  
617 find expression of Kv2 channels to be similar in mouse and human DRG. An overall similarity is  
618 supported by the presence of detectable Kv2 channels in most neurons, consistent with transcriptomics  
619 data from both mice and humans (Tavares-Ferreira et al., 2022; Zheng et al., 2019). The subcellular  
620 localization of Kv2 channels also appears similar between mice and humans. These similarities include  
621 enrichment of Kv2 channels at the outer edge of neurons, Kv2 clusters on the neuron soma as well as  
622 presence of Kv2.1 and Kv2.2 on DRG neuron axons. These similarities suggest that the functional roles of  
623 Kv2 channels could be similar in both mouse and human DRG neurons.

624

625 Overall, we find attributes of Kv2 channel localization in somatosensory neurons that could point to  
626 their functional roles in sensory information processing. The broad expression of Kv2.2 among DRG  
627 neuron types and expansive axonal localization of Kv2.2 suggest a key role for this channel in the  
628 somatosensory nervous system. The specialized divergence of Kv2.1 and Kv2.2 suggest the functional  
629 roles of Kv2 subtypes in DRG neurons are overlapping yet distinct.

630 REFERENCES

631

- 632 Bishop, H. I., Cobb, M. M., Kirmiz, M., Parajuli, L. K., Mandikian, D., Philp, A. M., . . . Trimmer, J.  
633 S. (2018). Kv2 ion channels determine the expression and localization of the associated  
634 AMIGO-1 cell adhesion molecule in adult brain neurons. *Front Mol Neurosci*, *11*, 1.  
635 doi:10.3389/fnmol.2018.00001
- 636 Bishop, H. I., Guan, D., Bocksteins, E., Parajuli, L. K., Murray, K. D., Cobb, M. M., . . . Trimmer, J.  
637 S. (2015). Distinct cell- and layer-specific expression patterns and independent  
638 regulation of Kv2 channel subtypes in cortical pyramidal neurons. *J Neurosci*, *35*(44),  
639 14922-14942. doi:10.1523/jneurosci.1897-15.2015
- 640 Blaine, J. T., & Ribera, A. B. (1998). Heteromultimeric potassium channels formed by members  
641 of the Kv2 subfamily. *J Neurosci*, *18*(23), 9585-9593. doi:10.1523/jneurosci.18-23-  
642 09585.1998
- 643 Bocksteins, E. (2016). Kv5, Kv6, Kv8, and Kv9 subunits: No simple silent bystanders. *J Gen  
644 Physiol*, *147*(2), 105-125. doi:10.1085/jgp.201511507
- 645 Bocksteins, E., Raes, A. L., Van de Vijver, G., Bruyns, T., Van Bogaert, P. P., & Snyders, D. J.  
646 (2009). Kv2.1 and silent Kv subunits underlie the delayed rectifier K<sup>+</sup> current in cultured  
647 small mouse DRG neurons. *Am J Physiol Cell Physiol*, *296*(6), C1271-1278.  
648 doi:10.1152/ajpcell.00088.2009
- 649 Cho, W. G., & Valtschanoff, J. G. (2008). Vanilloid receptor TRPV1-positive sensory afferents in  
650 the mouse ankle and knee joints. *Brain Res.*, *1219*, 59-65.  
651 doi:<https://doi.org/10.1016/j.brainres.2008.04.043>
- 652 Coggeshall, R. E. (1992). A consideration of neural counting methods. *Trends Neurosci*, *15*(1), 9-  
653 13. doi:10.1016/0166-2236(92)90339-a
- 654 Coggeshall, R. E., & Lekan, H. A. (1996). Methods for determining numbers of cells and  
655 synapses: a case for more uniform standards of review. *J Comp Neurol*, *364*(1), 6-15.  
656 doi:10.1002/(SICI)1096-9861(19960101)364:1<6::AID-CNE2>3.0.CO;2-9
- 657 Cotella, D., Hernandez-Enriquez, B., Wu, X., Li, R., Pan, Z., Leveille, J., . . . Sesti, F. (2012). Toxic  
658 role of K<sup>+</sup> channel oxidation in mammalian brain. *J Neurosci*, *32*(12), 4133-4144.  
659 doi:10.1523/jneurosci.6153-11.2012
- 660 Dirajlal, S., Pauers, L. E., & Stucky, C. L. (2003). Differential response properties of IB(4)-positive  
661 and -negative unmyelinated sensory neurons to protons and capsaicin. *J Neurophysiol*,  
662 *89*(1), 513-524. doi:10.1152/jn.00371.2002
- 663 Dong, X., Han, S., Zylka, M. J., Simon, M. I., & Anderson, D. J. (2001). A diverse family of GPCRs  
664 expressed in specific subsets of nociceptive sensory neurons. *Cell*, *106*(5), 619-632.  
665 doi:10.1016/s0092-8674(01)00483-4
- 666 Du, J., Tao-Cheng, J. H., Zerfas, P., & McBain, C. J. (1998). The K<sup>+</sup> channel, Kv2.1, is apposed to  
667 astrocytic processes and is associated with inhibitory postsynaptic membranes in  
668 hippocampal and cortical principal neurons and inhibitory interneurons. *Neuroscience*,  
669 *84*(1), 37-48. doi:[https://doi.org/10.1016/S0306-4522\(97\)00519-8](https://doi.org/10.1016/S0306-4522(97)00519-8)
- 670 Einheber, S., Zanazzi, G., Ching, W., Scherer, S., Milner, T. A., Peles, E., & Salzer, J. L. (1997). The  
671 axonal membrane protein Caspr, a homologue of neurexin IV, is a component of the

- 672 septate-like paranodal junctions that assemble during myelination. *J Cell Biol*, 139(6),  
673 1495-1506. doi:10.1083/jcb.139.6.1495
- 674 Fletcher, E. V., Simon, C. M., Pagiazitis, J. G., Chalif, J. I., Vukojicic, A., Drobac, E., . . . Mentis, G.  
675 Z. (2017). Reduced sensory synaptic excitation impairs motor neuron function via Kv2.1  
676 in spinal muscular atrophy. *Nat Neurosci*, 20(7), 905-916. doi:10.1038/nn.4561
- 677 Gravagna, N. G., Knoeckel, C. S., Taylor, A. D., Hultgren, B. A., & Ribera, A. B. (2008). Localization  
678 of Kv2.2 protein in *Xenopus laevis* embryos and tadpoles. *J Comp Neurol*, 510(5), 508-  
679 524. doi:10.1002/cne.21804
- 680 Ha, H. (1970). Axonal bifurcation in the dorsal root ganglion of the cat: a light and electron  
681 microscopic study. *J Comp Neurol*, 140(2), 227-240. doi:10.1002/cne.901400206
- 682 He, X. H., Zang, Y., Chen, X., Pang, R. P., Xu, J. T., Zhou, X., . . . Liu, X. G. (2010). TNF- $\alpha$   
683 contributes to up-regulation of Nav1.3 and Nav1.8 in DRG neurons following motor fiber  
684 injury. *Pain*, 151(2), 266-279. doi:10.1016/j.pain.2010.06.005
- 685 Hermanstynne, T. O., Kihira, Y., Misono, K., Deitchler, A., Yanagawa, Y., & Misonou, H. (2010).  
686 Immunolocalization of the voltage-gated potassium channel Kv2.2 in GABAergic neurons  
687 in the basal forebrain of rats and mice. *J Comp Neurol*, 518(21), 4298-4310.  
688 doi:10.1002/cne.22457
- 689 Hwang, P. M., Fotuhi, M., Brecht, D. S., Cunningham, A. M., & Snyder, S. H. (1993). Contrasting  
690 immunohistochemical localizations in rat brain of two novel K<sup>+</sup> channels of the Shab  
691 subfamily. *J Neurosci*, 13(4), 1569-1576. doi:10.1523/jneurosci.13-04-01569.1993
- 692 Hwang, P. M., Glatt, C. E., Brecht, D. S., Yellen, G., & Snyder, S. H. (1992). A novel K<sup>+</sup> channel with  
693 unique localizations in mammalian brain: molecular cloning and characterization.  
694 *Neuron*, 8(3), 473-481. doi:10.1016/0896-6273(92)90275-i
- 695 Irie, T. (2021). Essential role of somatic Kv2 channels in high-frequency firing in cartwheel cells  
696 of the dorsal cochlear nucleus. *eNeuro*, 8(3). doi:10.1523/eneuro.0515-20.2021
- 697 Jensen, C. S., Watanabe, S., Stas, J. I., Klaphaak, J., Yamane, A., Schmitt, N., . . . Misonou, H.  
698 (2017). Trafficking of Kv2.1 channels to the axon initial segment by a novel  
699 nonconventional secretory pathway. *J Neurosci*, 37(48), 11523-11536.  
700 doi:10.1523/jneurosci.3510-16.2017
- 701 Johnson, B., Leek, A. N., Sole, L., Maverick, E. E., Levine, T. P., & Tamkun, M. M. (2018). Kv2  
702 potassium channels form endoplasmic reticulum/plasma membrane junctions via  
703 interaction with VAPA and VAPB. *Proc Natl Acad Sci U S A*, 115(31), E7331-e7340.  
704 doi:10.1073/pnas.1805757115
- 705 Johnston, J., Griffin, S. J., Baker, C., Skrzypiec, A., Chernova, T., & Forsythe, I. D. (2008). Initial  
706 segment Kv2.2 channels mediate a slow delayed rectifier and maintain high frequency  
707 action potential firing in medial nucleus of the trapezoid body neurons. *J Physiol*,  
708 586(14), 3493-3509. doi:10.1113/jphysiol.2008.153734
- 709 Kihira, Y., Hermanstynne, T. O., & Misonou, H. (2010). Formation of heteromeric Kv2 channels in  
710 mammalian brain neurons. *J Biol Chem*, 285(20), 15048-15055.  
711 doi:10.1074/jbc.M109.074260
- 712 Kim, K. X., & Rutherford, M. A. (2016). Maturation of NaV and Kv channel topographies in the  
713 auditory nerve spike initiator before and after developmental onset of hearing function.  
714 *J Neurosci*, 36(7), 2111-2118. doi:10.1523/jneurosci.3437-15.2016

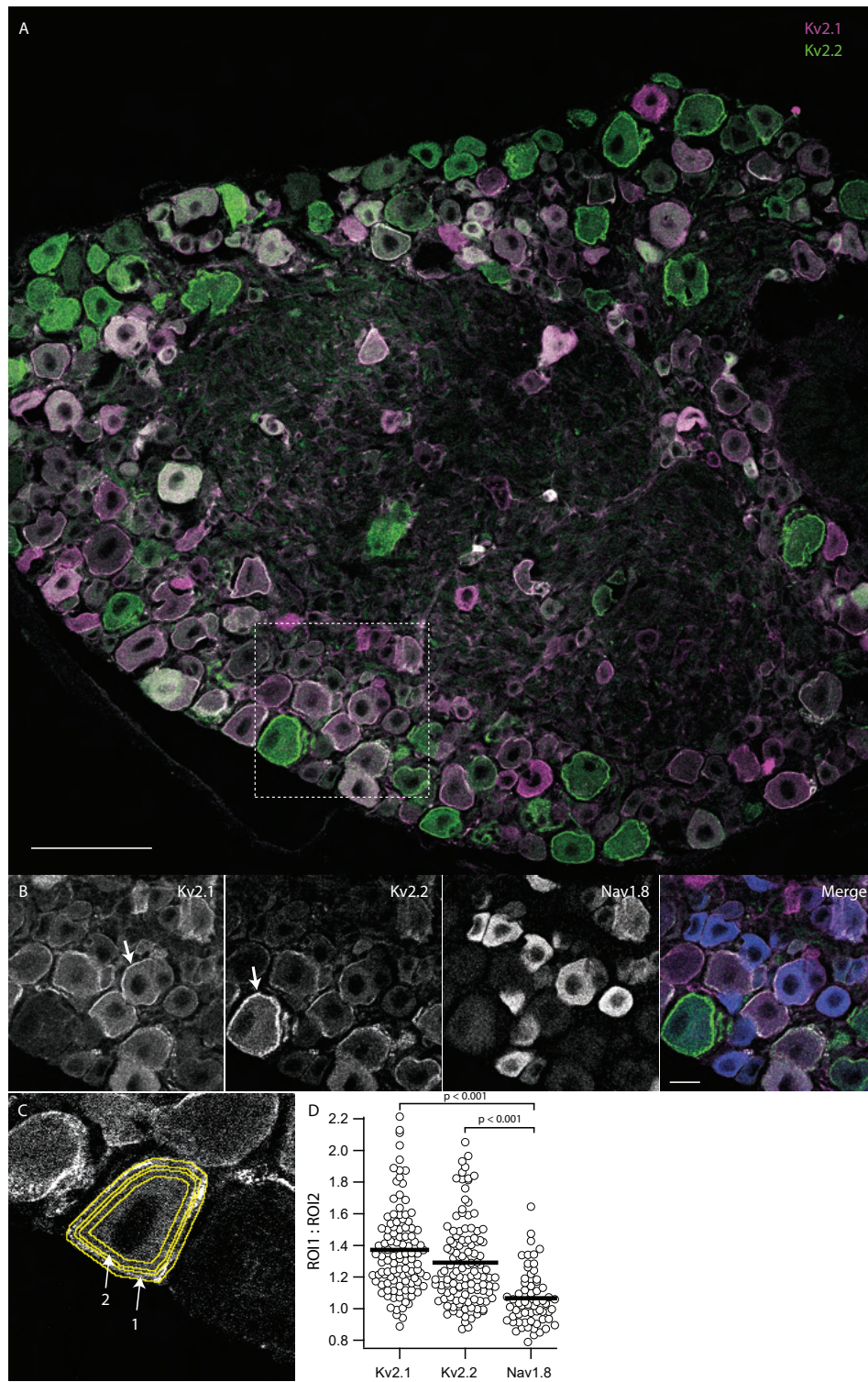
- 715 King, A. N., Manning, C. F., & Trimmer, J. S. (2014). A unique ion channel clustering domain on  
716 the axon initial segment of mammalian neurons. *J Comp Neurol*, *522*(11), 2594-2608.  
717 doi:10.1002/cne.23551
- 718 Kirmiz, M., Vierra, N. C., Palacio, S., & Trimmer, J. S. (2018). Identification of VAPA and VAPB as  
719 Kv2 channel-interacting proteins defining endoplasmic reticulum-plasma membrane  
720 junctions in mammalian brain neurons. *J Neurosci*. doi:10.1523/jneurosci.0893-18.2018
- 721 Lee, M. C., Nahorski, M. S., Hockley, J. R. F., Lu, V. B., Ison, G., Pattison, L. A., . . . Woods, C. G.  
722 (2020). Human labor pain is influenced by the voltage-gated potassium channel Kv 6.4  
723 subunit. *Cell Rep*, *32*(3), 107941. doi:10.1016/j.celrep.2020.107941
- 724 Legland, D., Arganda-Carreras, I., & Andrey, P. (2016). MorphoLibJ: integrated library and  
725 plugins for mathematical morphology with ImageJ. *Bioinformatics*, *32*(22), 3532-3534.  
726 doi:10.1093/bioinformatics/btw413
- 727 Li, X. N., Herrington, J., Petrov, A., Ge, L., Eiermann, G., Xiong, Y., . . . Zhou, Y. P. (2013). The role  
728 of voltage-gated potassium channels Kv2.1 and Kv2.2 in the regulation of insulin and  
729 somatostatin release from pancreatic islets. *J Pharmacol Exp Ther*, *344*(2), 407-416.  
730 doi:10.1124/jpet.112.199083
- 731 Lim, S. T., Antonucci, D. E., Scannevin, R. H., & Trimmer, J. S. (2000). A novel targeting signal for  
732 proximal clustering of the Kv2.1 K<sup>+</sup> channel in hippocampal neurons. *Neuron*, *25*(2), 385-  
733 397. doi:10.1016/s0896-6273(00)80902-2
- 734 Liu, P. W., & Bean, B. P. (2014). Kv2 channel regulation of action potential repolarization and  
735 firing patterns in superior cervical ganglion neurons and hippocampal CA1 pyramidal  
736 neurons. *J Neurosci*, *34*(14), 4991-5002. doi:10.1523/jneurosci.1925-13.2014
- 737 Matsuda, S., Kobayashi, N., Terashita, T., Shimokawa, T., Shigemoto, K., Mominoki, K., . . .  
738 Fujiwara, T. (2005). Phylogenetic investigation of Dogiel's pericellular nests and Cajal's  
739 initial glomeruli in the dorsal root ganglion. *J Comp Neurol*, *491*(3), 234-245.  
740 doi:10.1002/cne.20713
- 741 Misonou, H., Mohapatra, D. P., Menegola, M., & Trimmer, J. S. (2005). Calcium- and metabolic  
742 state-dependent modulation of the voltage-dependent Kv2.1 channel regulates  
743 neuronal excitability in response to ischemia. *J Neurosci*, *25*(48), 11184-11193.  
744 doi:10.1523/jneurosci.3370-05.2005
- 745 Muennich, E. A., & Fyffe, R. E. (2004). Focal aggregation of voltage-gated, Kv2.1 subunit-  
746 containing, potassium channels at synaptic sites in rat spinal motoneurons. *J Physiol*,  
747 *554*(Pt 3), 673-685. doi:10.1113/jphysiol.2003.056192
- 748 Newkirk, G. S., Guan, D., Dembrow, N., Armstrong, W. E., Foehring, R. C., & Spain, W. J. (2022).  
749 Kv2.1 potassium channels regulate repetitive burst firing in extratelencephalic  
750 neocortical pyramidal neurons. *Cereb Cortex*, *32*(5), 1055-1076.  
751 doi:10.1093/cercor/bhab266
- 752 Panzera, L. C., Johnson, B., Quinn, J. A., Cho, I. H., Tamkun, M. M., & Hoppa, M. B. (2022).  
753 Activity-dependent endoplasmic reticulum Ca<sup>2+</sup> uptake depends on Kv2.1-mediated  
754 endoplasmic reticulum/plasma membrane junctions to promote synaptic transmission.  
755 *Proc Natl Acad Sci U S A*, *119*(30), e2117135119. doi:10.1073/pnas.2117135119
- 756 Rasband, M. N., Trimmer, J. S., Schwarz, T. L., Levinson, S. R., Ellisman, M. H., Schachner, M., &  
757 Shrager, P. (1998). Potassium channel distribution, clustering, and function in

- 758 remyelinating rat axons. *J Neurosci*, 18(1), 36-47. doi:10.1523/jneurosci.18-01-  
759 00036.1998
- 760 Regnier, G., Bocksteins, E., Van de Vijver, G., Snyders, D. J., & van Bogaert, P. P. (2016). The  
761 contribution of Kv2.2-mediated currents decreases during the postnatal development of  
762 mouse dorsal root ganglion neurons. *Physiol Rep*, 4(6). doi:10.14814/phy2.12731
- 763 Romer, S. H., Dominguez, K. M., Gelpi, M. W., Deardorff, A. S., Tracy, R. C., & Fyffe, R. E. W.  
764 (2014). Redistribution of Kv2.1 ion channels on spinal motoneurons following peripheral  
765 nerve injury. *Brain research*, 1547, 1-15. doi:10.1016/j.brainres.2013.12.012
- 766 Sarmiere, P. D., Weigle, C. M., & Tamkun, M. M. (2008). The Kv2.1 K<sup>+</sup> channel targets to the  
767 axon initial segment of hippocampal and cortical neurons in culture and in situ. *BMC*  
768 *Neurosci*, 9, 112. doi:10.1186/1471-2202-9-112
- 769 Scannevin, R. H., Murakoshi, H., Rhodes, K. J., & Trimmer, J. S. (1996). Identification of a  
770 cytoplasmic domain important in the polarized expression and clustering of the Kv2.1 K<sup>+</sup>  
771 channel. *J Cell Biol*, 135(6 Pt 1), 1619-1632. doi:10.1083/jcb.135.6.1619
- 772 Schindelin, J., Arganda-Carreras, I., Frise, E., Kaynig, V., Longair, M., Pietzsch, T., . . . Cardona, A.  
773 (2012). Fiji: an open-source platform for biological-image analysis. *Nat Methods*, 9(7),  
774 676-682. doi:10.1038/nmeth.2019
- 775 Scott, B., Leu, J., & Cinader, B. (1988). Effects of aging on neuronal electrical membrane  
776 properties. *Mech Ageing Dev*, 44(3), 203-214. doi:10.1016/0047-6374(88)90022-x
- 777 Shields, S. D., Ahn, H. S., Yang, Y., Han, C., Seal, R. P., Wood, J. N., . . . Dib-Hajj, S. D. (2012).  
778 Nav1.8 expression is not restricted to nociceptors in mouse peripheral nervous system.  
779 *Pain*, 153(10), 2017-2030. doi:10.1016/j.pain.2012.04.022
- 780 Shiers, S., Klein, R. M., & Price, T. J. (2020). Quantitative differences in neuronal subpopulations  
781 between mouse and human dorsal root ganglia demonstrated with RNAscope in situ  
782 hybridization. *Pain*, 161(10), 2410-2424. doi:10.1097/j.pain.0000000000001973
- 783 Shiers, S., Sankaranarayanan, I., Jeevakumar, V., Cervantes, A., Reese, J. C., & Price, T. J. (2021).  
784 Convergence of peptidergic and non-peptidergic protein markers in the human dorsal  
785 root ganglion and spinal dorsal horn. *J Comp Neurol*, 529(10), 2771-2788.  
786 doi:10.1002/cne.25122
- 787 Sun, Z. W., Waybright, J. M., Beldar, S., Chen, L., Foley, C. A., Norris-Drouin, J. L., . . . Wang, Y.  
788 (2022). Cdy1 deficiency brakes neuronal excitability and nociception through promoting  
789 Kcnb1 transcription in peripheral sensory neurons. *Adv Sci (Weinh)*, 9(10), e2104317.  
790 doi:10.1002/advs.202104317
- 791 Tavares-Ferreira, D., Shiers, S., Ray, P. R., Wangzhou, A., Jeevakumar, V., Sankaranarayanan, I., .  
792 . . Price, T. J. (2022). Spatial transcriptomics of dorsal root ganglia identifies molecular  
793 signatures of human nociceptors. *Sci Transl Med*, 14(632), eabj8186.  
794 doi:10.1126/scitranslmed.abj8186
- 795 Thapa, P., Stewart, R., Sepela, R. J., Vivas, O., Parajuli, L. K., Lillya, M., . . . Sack, J. T. (2021).  
796 EVAP: A two-photon imaging tool to study conformational changes in endogenous Kv2  
797 channels in live tissues. *J Gen Physiol*, 153(11). doi:10.1085/jgp.202012858
- 798 Trimmer, J. S. (1991). Immunological identification and characterization of a delayed rectifier K<sup>+</sup>  
799 channel polypeptide in rat brain. *Proc Natl Acad Sci U S A*, 88(23), 10764-10768.  
800 doi:10.1073/pnas.88.23.10764

- 801 Tsantoulas, C., Zhu, L., Shaifta, Y., Grist, J., Ward, J. P., Raouf, R., . . . McMahon, S. B. (2012).  
802 Sensory neuron downregulation of the Kv9.1 potassium channel subunit mediates  
803 neuropathic pain following nerve injury. *J Neurosci*, *32*(48), 17502-17513.  
804 doi:10.1523/jneurosci.3561-12.2012
- 805 Tsantoulas, C., Zhu, L., Yip, P., Grist, J., Michael, G. J., & McMahon, S. B. (2014). Kv2 dysfunction  
806 after peripheral axotomy enhances sensory neuron responsiveness to sustained input.  
807 *Exp Neurol*, *251*, 115-126. doi:10.1016/j.expneurol.2013.11.011
- 808 Usoskin, D., Furlan, A., Islam, S., Abdo, H., Lönnnerberg, P., Lou, D., . . . Ernfors, P. (2015).  
809 Unbiased classification of sensory neuron types by large-scale single-cell RNA  
810 sequencing. *Nat Neurosci*, *18*(1), 145-153. doi:10.1038/nn.3881
- 811 Valtcheva, M. V., Copits, B. A., Davidson, S., Sheahan, T. D., Pullen, M. Y., McCall, J. G., . . .  
812 Gereau, R. W. t. (2016). Surgical extraction of human dorsal root ganglia from organ  
813 donors and preparation of primary sensory neuron cultures. *Nat Protoc*, *11*(10), 1877-  
814 1888. doi:10.1038/nprot.2016.111
- 815 Vierra, N. C., O'Dwyer, S. C., Matsumoto, C., Santana, L. F., & Trimmer, J. S. (2021). Regulation  
816 of neuronal excitation-transcription coupling by Kv2.1-induced clustering of somatic L-  
817 type Ca(2+) channels at ER-PM junctions. *Proc Natl Acad Sci U S A*, *118*(46).  
818 doi:10.1073/pnas.2110094118
- 819 Vullhorst, D., Mitchell, R. M., Keating, C., Roychowdhury, S., Karavanova, I., Tao-Cheng, J. H., &  
820 Buonanno, A. (2015). A negative feedback loop controls NMDA receptor function in  
821 cortical interneurons via neuregulin 2/ErbB4 signalling. *Nat Commun*, *6*, 7222.  
822 doi:10.1038/ncomms8222
- 823 Wang, H., & Zylka, M. J. (2009). Mrgprd-expressing polymodal nociceptive neurons innervate  
824 most known classes of substantia gelatinosa neurons. *J Neurosci*, *29*(42), 13202-13209.  
825 doi:10.1523/jneurosci.3248-09.2009
- 826 Wangzhou, A., McIlvried, L. A., Paige, C., Barragan-Iglesias, P., Shiers, S., Ahmad, A., . . . Price, T.  
827 J. (2020). Pharmacological target-focused transcriptomic analysis of native vs cultured  
828 human and mouse dorsal root ganglia. *Pain*, *161*(7), 1497-1517.  
829 doi:10.1097/j.pain.0000000000001866
- 830 Zheng, Y., Liu, P., Bai, L., Trimmer, J. S., Bean, B. P., & Ginty, D. D. (2019). Deep sequencing of  
831 somatosensory neurons reveals molecular determinants of intrinsic physiological  
832 properties. *Neuron*, *103*(4), 598-616.e597. doi:10.1016/j.neuron.2019.05.039  
833

834 FIGURES AND FIGURE LEGENDS

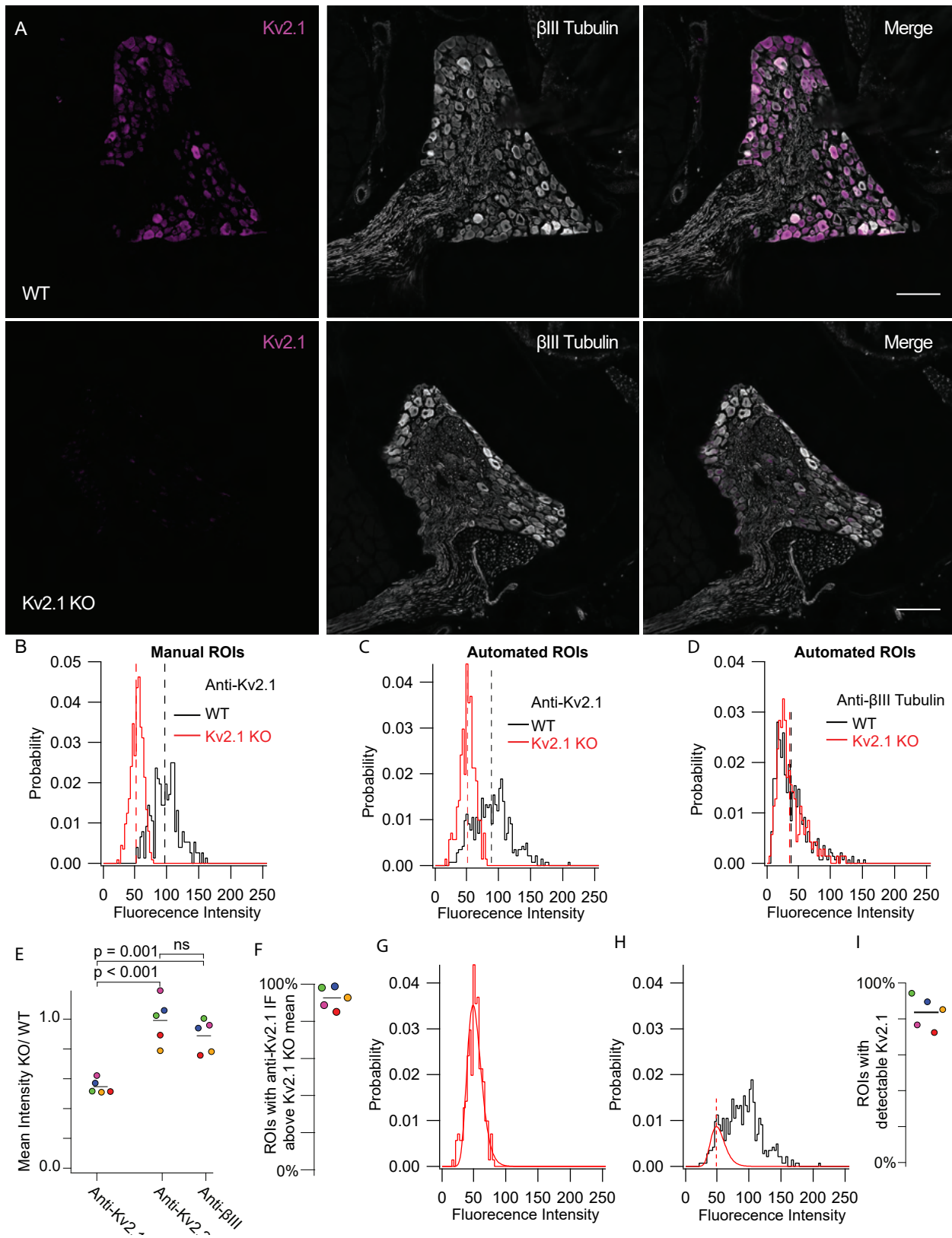
835 Figure 1



837 **Figure 1 legend**

838 Kv2.1 and Kv2.2 protein are enriched at the outer edge of DRG neuron somas relative to  
839 Nav1.8. Lumbar DRG section from an 11 week old male mouse labeled with antibodies which  
840 target Kv2.1, Kv2.2 or Nav1.8. **A**, Anti-Kv2.1 (magenta) and anti-Kv2.2 (green)  
841 immunofluorescence in a lumbar DRG section. Scale bar is 100  $\mu\text{m}$ . **B**, Anti-Kv2.1, anti-Kv2.2 and  
842 anti-Nav1.8 immunofluorescence from box shown in A. Arrows indicate prominent localization  
843 of anti-Kv2 immunofluorescence at the edge of DRG neuron somas. In merge image anti-Kv2.1,  
844 anti-Kv2.2 and anti-Nav1.8 immunofluorescence is magenta, green and blue respectively. Scale  
845 bar is 20  $\mu\text{m}$ . **C**, Representative ROIs that encompass the outer edge of DRG neurons (arrow 1)  
846 and the region just inside the outer edge (arrow 2). **D**, Ratio of anti-Kv2.1, anti-Kv2.2 or anti-  
847 Nav1.8 immunofluorescence from outer and inner ROIs for individual neurons from image in A.  
848 Bars represent mean. One-way ANOVA  $p < 0.001$ .  $p$  values in figure represent post hoc Tukey's  
849 test.  $N = 1$  mouse,  $n = 124$  neurons. Detailed information on mouse used can be found in table  
850 1.

851 **Figure 2**

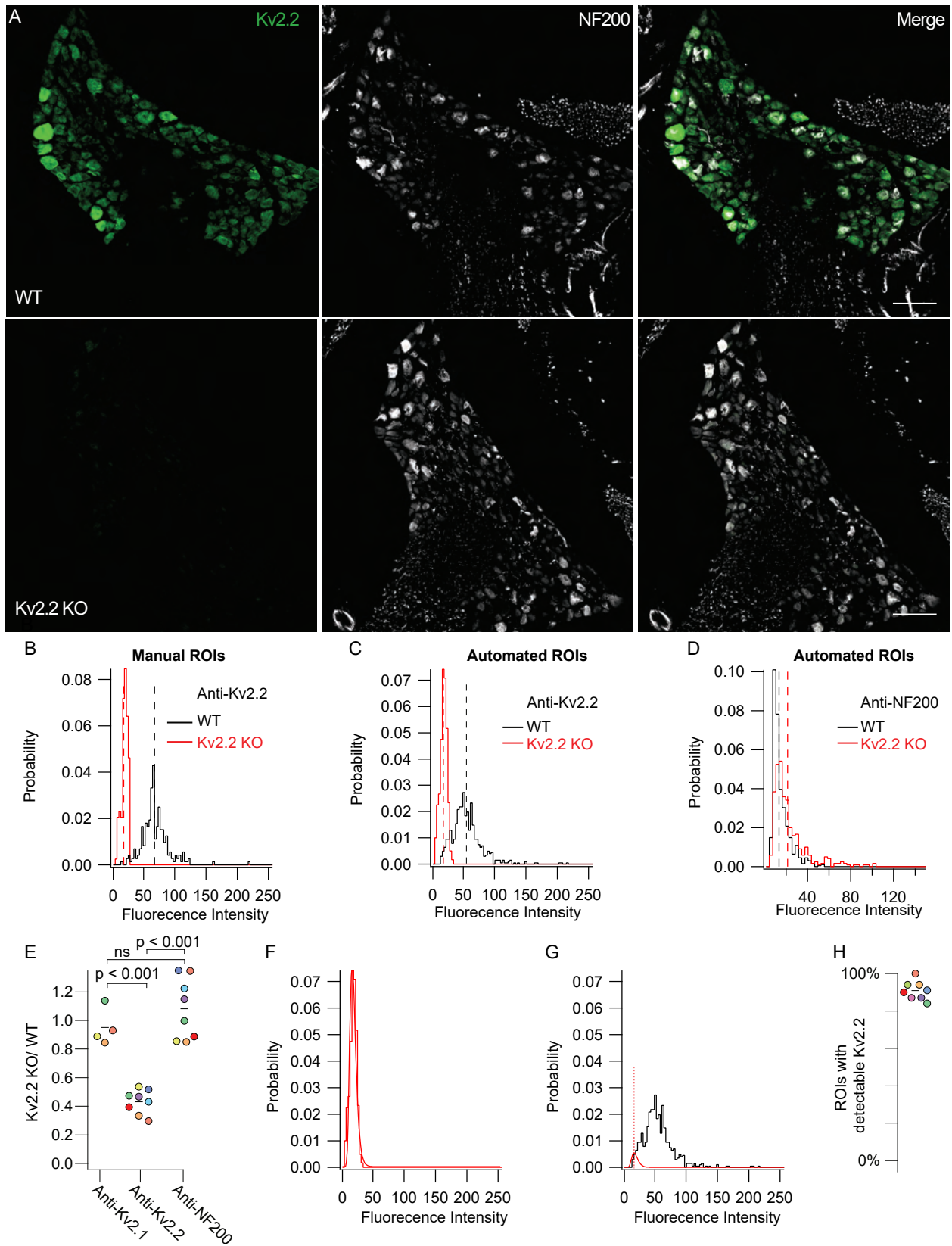


853 **Figure 2 legend**

854 Kv2.1 protein is detectable in mouse DRG neurons. **A**, WT (top) and Kv2.1 KO (bottom) DRG  
855 sections taken from 7 week old female mice from the 13<sup>th</sup> thoracic DRG immunolabeled for  
856 Kv2.1 (magenta) and BIII tubulin (white). Images were taken with identical imaging settings and  
857 are set to the same brightness and contrast. Scale bars are 100  $\mu$ m. **B**, Distribution of  
858 fluorescence intensity from manual analysis of WT (black) and Kv2.1 KO (red) neurons. Dotted  
859 lines represent mean. Data represent fluorescence intensity of 254 WT profiles from 10 DRG  
860 sections from 1 mouse or 375 Kv2.1 KO profiles from 5 DRG sections from 1 mouse. Images  
861 shown in A represent one section from WT and Kv2.1 KO mice used in this data set. **C**,  
862 Distribution of fluorescence intensity from automated analysis of the same data set shown in B.  
863 Dotted lines represent mean. Data represent fluorescence intensity of 476 WT or 576 Kv2.1 KO  
864 profiles selected by automated analysis method. **D**, Distribution of BIII tubulin fluorescence  
865 intensity from the same WT (black) and Kv2.1 KO (red) profiles shown in C. Dotted lines  
866 represent mean. **E**, Mean fluorescence intensity of Kv2.1 KO neurons normalized to WT neurons  
867 labeled with anti-Kv2.1, anti-Kv2.2 and anti-BIII tubulin antibodies. Each point represents one  
868 Kv2.1 KO mouse normalized to one age and sex matched WT mouse which was stained  
869 simultaneously and imaged with identical microscopy settings. The color of each point  
870 represents the same mouse and purple points represent data from the mouse whose DRG  
871 immunofluorescence data are shown in A, B, C and D. one-way ANOVA  $p < 0.001$ .  $p$  values in  
872 figure represent post hoc Tukey's test. **F**, Percentage of ROIs with anti-Kv2.1  
873 immunofluorescence above the mean immunofluorescence of 5 mice (1 female and 4 male).  
874 Point colors correspond to the WT mice analyzed in E. All mice were compared to age and sex

875 matched Kv2.1 KO mice. N = 5 WT and 5 Kv2.1 KO mice. **G**, Kv2.1 KO data shown in B fit with a  
876 log normal distribution (red fit). **H**, WT data shown in B fit with the Kv2.1 KO distribution (red  
877 fit) where width and mean were constrained to the Kv2.1 KO distribution and amplitude was  
878 unconstrained (equation 1). Red dotted line represents the mean of the Kv2.1 KO distribution.  
879 Only WT data to the left of red dotted line was used for the fit. **I**, Percentage of ROIs with  
880 detectable Kv2.1 protein of 5 mice (1 female and 4 males). Point colors correspond to the WT  
881 mice analyzed in E. All mice were compared to age and sex matched Kv2.1 KO mice. N = 5 WT  
882 and 5 Kv2.1 KO mice. Detailed information on each mouse used can be found in table 1.  
883

884 **Figure 3**



886 **Figure 3 legend**

887 Kv2.2 protein is detectable in mouse DRG neurons. **A**, WT (top) and Kv2.2 KO (bottom) DRG  
888 sections from the 13<sup>th</sup> thoracic DRG in 7 week old male mice immunolabeled for Kv2.2 (green)  
889 and NF200 (white). Identical imaging and display settings. Scale bars are 100  $\mu$ m. **B**,  
890 Distribution of fluorescence intensities from manual analysis of WT (black) and Kv2.2 KO (red)  
891 profiles. Dotted lines represent mean. Data represents fluorescence intensities from 241 WT  
892 profiles from 11 DRG sections and 1 mouse or 130 Kv2.2 KO profiles from 6 DRG sections and 1  
893 mouse. Images shown in A represent one section from WT and Kv2.1 KO mice used in this data  
894 set. **C**, Distribution of fluorescence intensity from automated analysis of the same data set  
895 shown in B. Dotted lines represent mean. Data represent fluorescence intensity of 673 WT or  
896 400 Kv2.2 KO profiles selected by automated analysis method. **D**, Distribution of anti-NF200  
897 immunofluorescence intensity from the same WT (black) and Kv2.2 KO (red) neurons shown in  
898 B. Dotted lines represent mean. **E**, Mean fluorescence intensity of Kv2.2 KO ROIs normalized to  
899 WT neurons labeled with anti-Kv2.1, anti-Kv2.2 and anti-NF200 antibodies. Each point  
900 represents one Kv2.2 KO mouse normalized to one age and sex matched WT mouse which was  
901 stained simultaneously and imaged with identical microscopy settings. The color of each point  
902 represents the same mouse and purple points represent data from the male mouse whose DRG  
903 immunofluorescence data are shown in A, B and C. Missing points in anti-Kv2.1 column are  
904 because some sections were not labeled with anti-Kv2.1 antibodies. one-way ANOVA  $p < 0.001$ .  
905  $p$  values in figure represent Tukey's post hoc test. **F**, Kv2.2 KO data shown in B fit with a log  
906 normal distribution (red fit). **G**, WT data shown in B fit with the Kv2.2 KO distribution (red fit)  
907 where width and mean were constrained to the Kv2.2 KO distribution and amplitude was

908 unconstrained (equation 1). Red dotted line represents the mean of the Kv2.2 KO distribution.

909 Only WT data to the left of red dotted line was used for the fit. **H**, Percentage of ROIs with

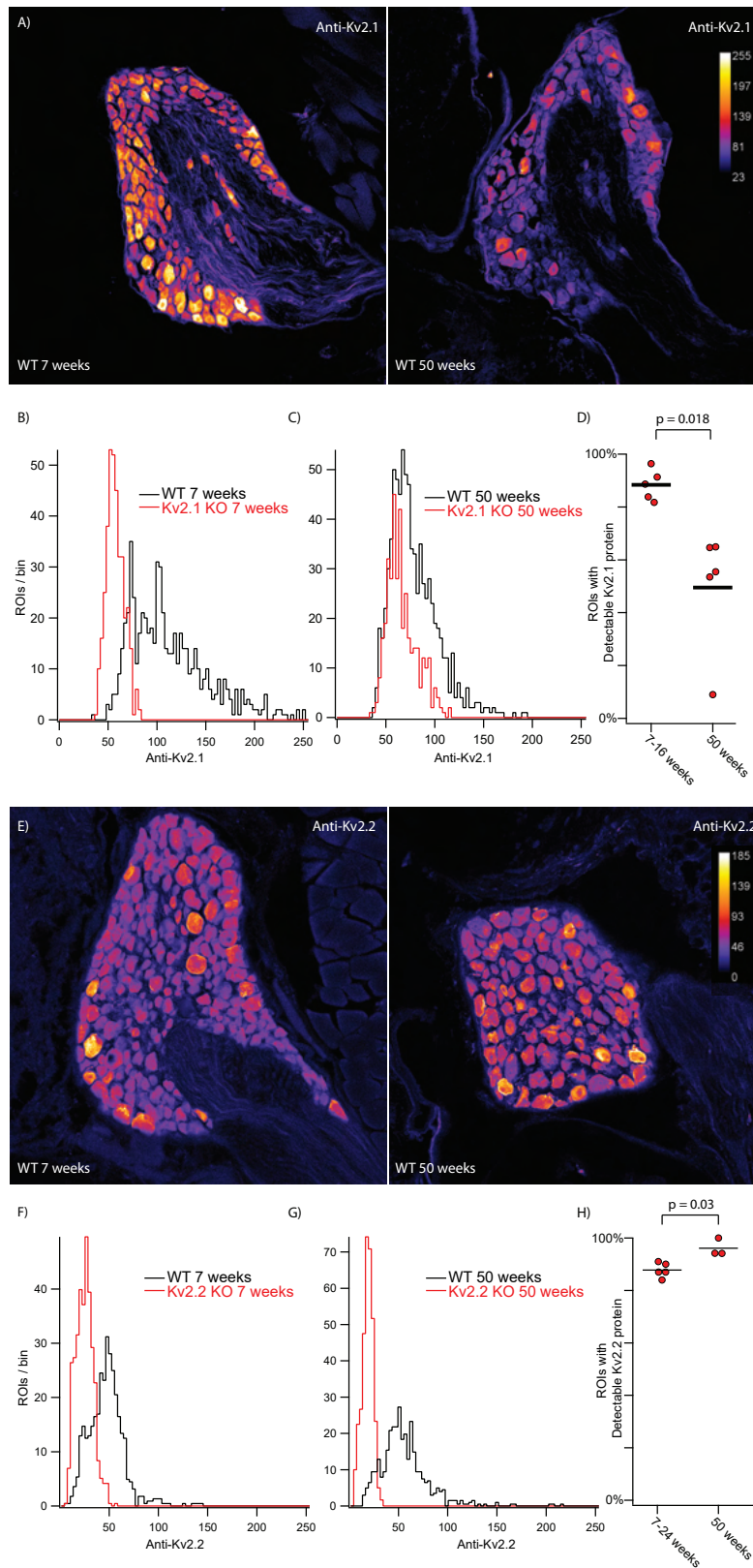
910 detectable Kv2.2 protein of 8 mice (7 males and 1 female). Point colors correspond to the WT

911 mice analyzed in D. All mice were compared to age and sex matched Kv2.2 KO mice. N = 8 WT

912 and 8 Kv2.2 KO mice. Detailed information on each mouse used can be found in table 1.

913

914 **Figure 4**



916 **Figure 4 legend**

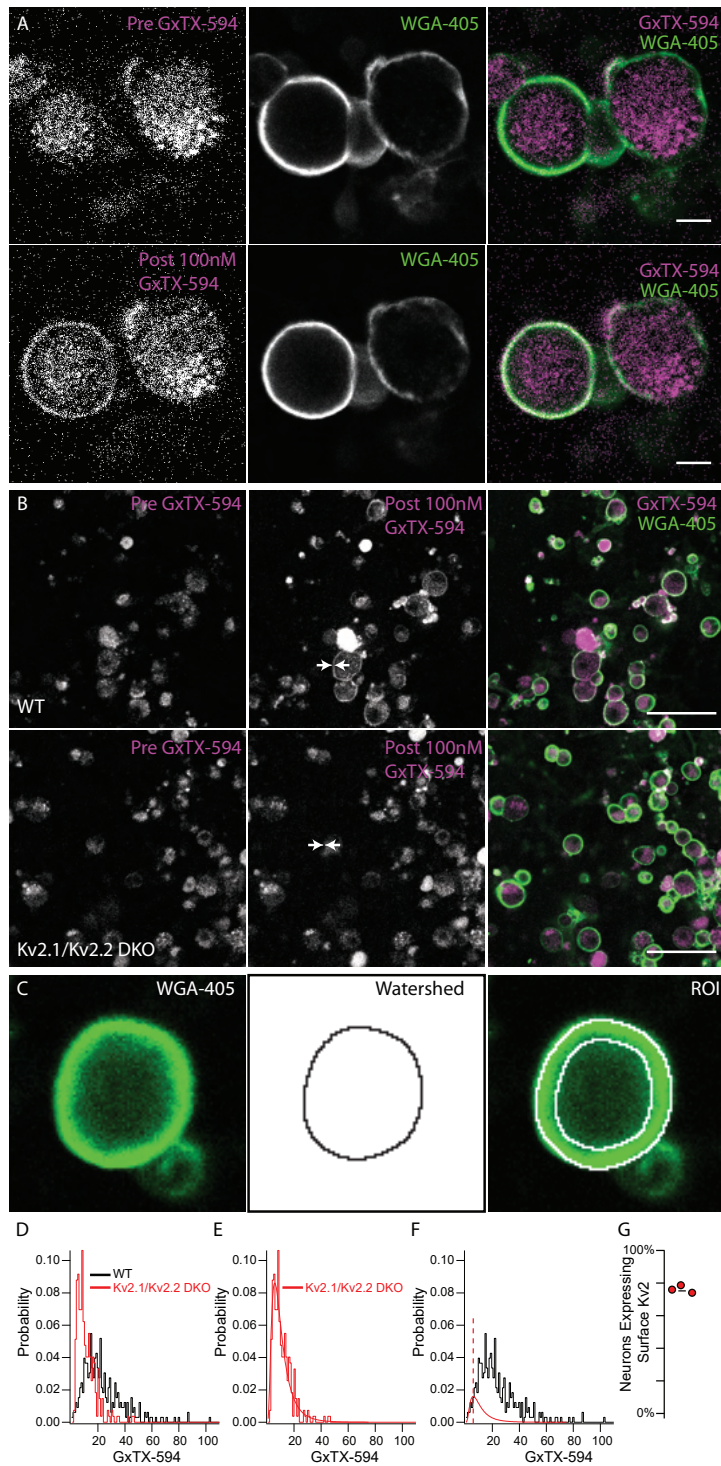
917 Detectable Kv2.1 protein decreases in older mice while detectable Kv2.2 does not. **A**, DRG  
918 sections from the 13<sup>th</sup> thoracic DRG in 7 week (left) and 50 week (right) old mice  
919 immunolabeled for Kv2.1. Vertical bar on right is pseudo coloring key for pixel intensity.  
920 Identical imaging and display settings. Scale bars are 100  $\mu$ m. **B**, Distribution of fluorescence  
921 intensities from 7 week old WT (black) and 7 week old Kv2.1 KO (red) ROIs generated by  
922 automated method. 609 WT ROIs from 1 mouse. 367 Kv2.1 KO ROIs from 1 mouse. **C**,  
923 Distribution of fluorescence intensities from 50 week old WT (black) and 50 week old Kv2.1 KO  
924 (red) ROIs. 793 WT ROIs from 1 mouse. 378 Kv2.1 KO ROIs from 1 mouse. **D**, Percentage of ROIs  
925 with detectable Kv2.1 protein in 7-16 week old and 50 week old mice. Data from 7-16 week old  
926 mice is the same data in Figure 2. N = 4 mice 7 weeks old and 1 mouse 16 weeks old and N = 5  
927 mice 50 weeks old. Detailed information on each mouse used can be found in table 1. **E**, DRG  
928 sections from the 13th thoracic DRG in 7 week (left) and 50 week (right) old mice  
929 immunolabeled for Kv2.2. Vertical bar on right is pseudo coloring key for pixel intensity.  
930 Identical imaging and display settings. Scale bars are 100  $\mu$ m. **F**, Distribution of fluorescence  
931 intensities from 7 week old WT (black) and 7 week old Kv2.2 KO (red) ROIs generated by  
932 automated method. 746 WT ROIs from 1 mouse. 717 Kv2.2 KO ROIs from 1 mouse. Data from  
933 same mice shown in E. **G**, Distribution of fluorescence intensities from 50 week old WT (black)  
934 and 50 week old Kv2.2 KO (red) ROIs generated by automated method. 671 WT ROIs from 1  
935 mouse. 398 Kv2.2 KO ROIs from 1 mouse. Data from same mice shown in E. **H**, Percentage of  
936 ROIs with detectable Kv2.2 protein in 7-24 week old and 50 week old mice. Data is the same  
937 data from Figure 3 where mice were separated into a young group (7-24 weeks) and an old

938 group (50 weeks). N = 3 mice 7 weeks old, 1 mouse 24 weeks old and 1 mouse 25 weeks old. N

939 = 3 mice 50 weeks old. Detailed information on each mouse used can be found in table 1.

940

941 **Figure 5**



942

943 **Figure 5 legend**

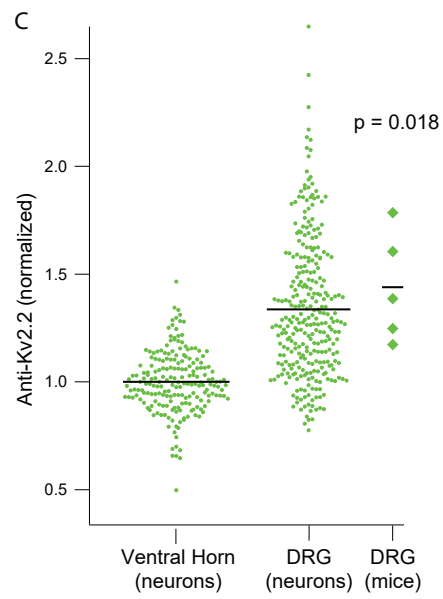
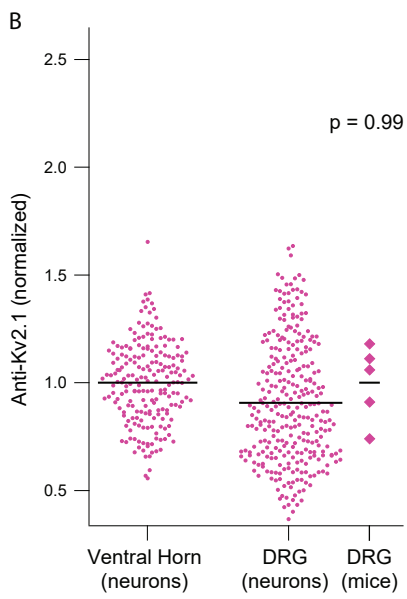
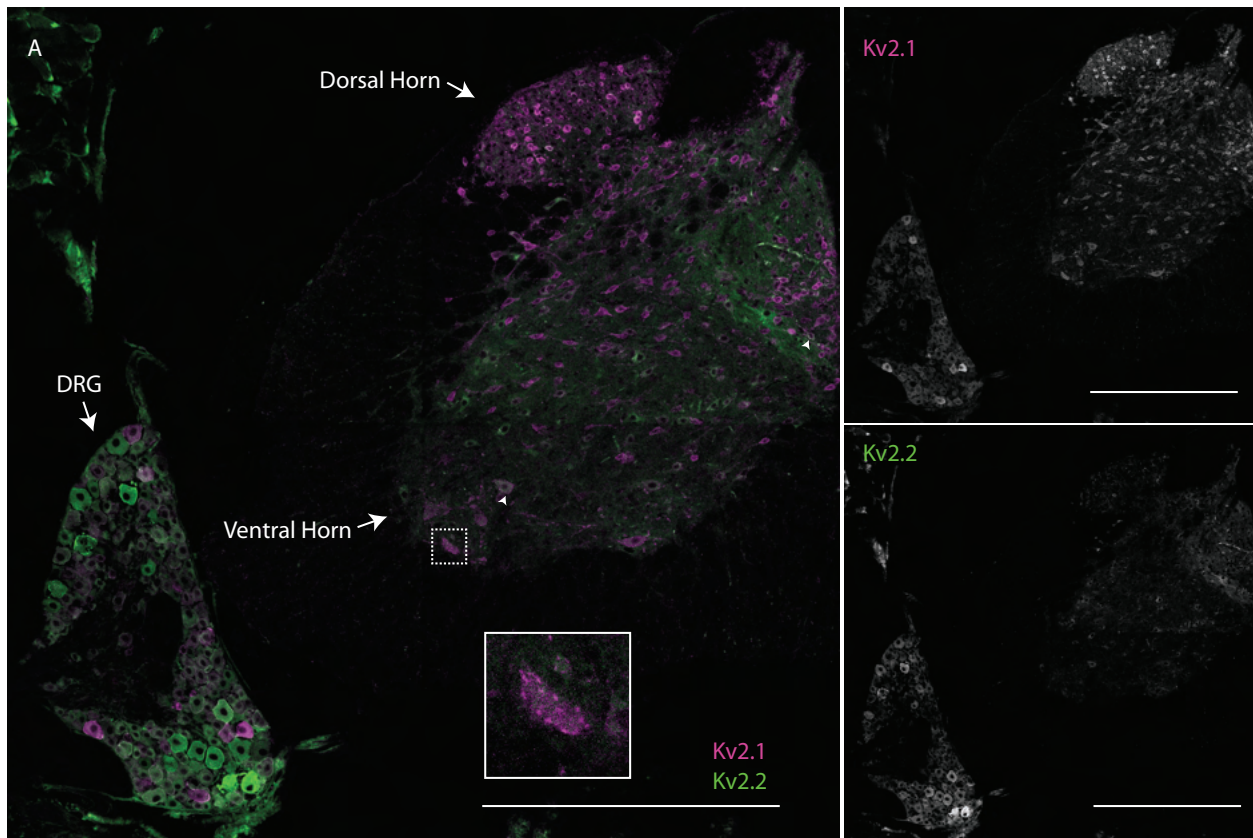
944 Kv2 channels are expressed at the surface membrane of DRG neurons. **A**, Fluorescence of live  
945 dissociated DRG neurons excited at 594 nm before (top left) and after (bottom left) application  
946 of 100 nM GxTX-594. Fluorescence from membrane marker WGA-405 before (top middle) and  
947 after application of 100 nM GxTX-594 (bottom middle). Merge image shows 594 excitation  
948 fluorescence (magenta) and 405 excitation fluorescence (green). Scale bar 20  $\mu\text{m}$ . **B**,  
949 Dissociated DRG neurons from WT (top) and Kv2.1/Kv2.2 DKO (bottom) mice before and after  
950 the application of GxTX-594, left panel and middle panel respectively. Arrows in middle panel  
951 indicate location of surface membrane based on WGA-405 fluorescence. Right images are  
952 merge of 594 excitation fluorescence (magenta) and 405 excitation fluorescence (green) after  
953 application of 100 nM GxTX-594. Scale bars 100  $\mu\text{m}$ . **C**, Example of WGA-405 fluorescence (left)  
954 used in watershed segmentation (middle) to generate annulus ROI (right) used to analyze  
955 fluorescence intensity at the membrane. **D**, Distribution of fluorescence intensity from WT  
956 (black) and Kv2.1/Kv2.2 DKO (red) neurons. Data represents the fluorescence intensity of 326  
957 WT neurons from 1 mouse or 271 Kv2.1/Kv2.2 DKO neurons from 1 mouse. DRG from all levels  
958 of the spinal cord were pooled. **E**, Kv2.1/Kv2.2 DKO data shown in D fit with a log normal  
959 distribution (red fit). **F**, WT data shown in D fit with the Kv2.1/Kv2.2 DKO distribution (red fit)  
960 where width and mean were constrained to the Kv2.1/Kv2.2 DKO distribution and amplitude  
961 was unconstrained (equation 1). Red dotted line represents the mean of the Kv2.1/Kv2.2 DKO  
962 distribution. Only WT data to the left of red dotted line was used for the fit. **G**, Percentage of  
963 neurons with detectable surface Kv2 protein, from an experiment where one WT mouse was  
964 compared to one DKO mouse and an identical experiment where two WT mice were compared

965 to one DKO mouse (N=3 WT mice N=2 Kv2.1/Kv2.2 DKO mice). N = 3 WT mice and N = 2 DKO

966 mice. Detailed information on each mouse used can be found in table 1.

967

968 **Figure 6**



969

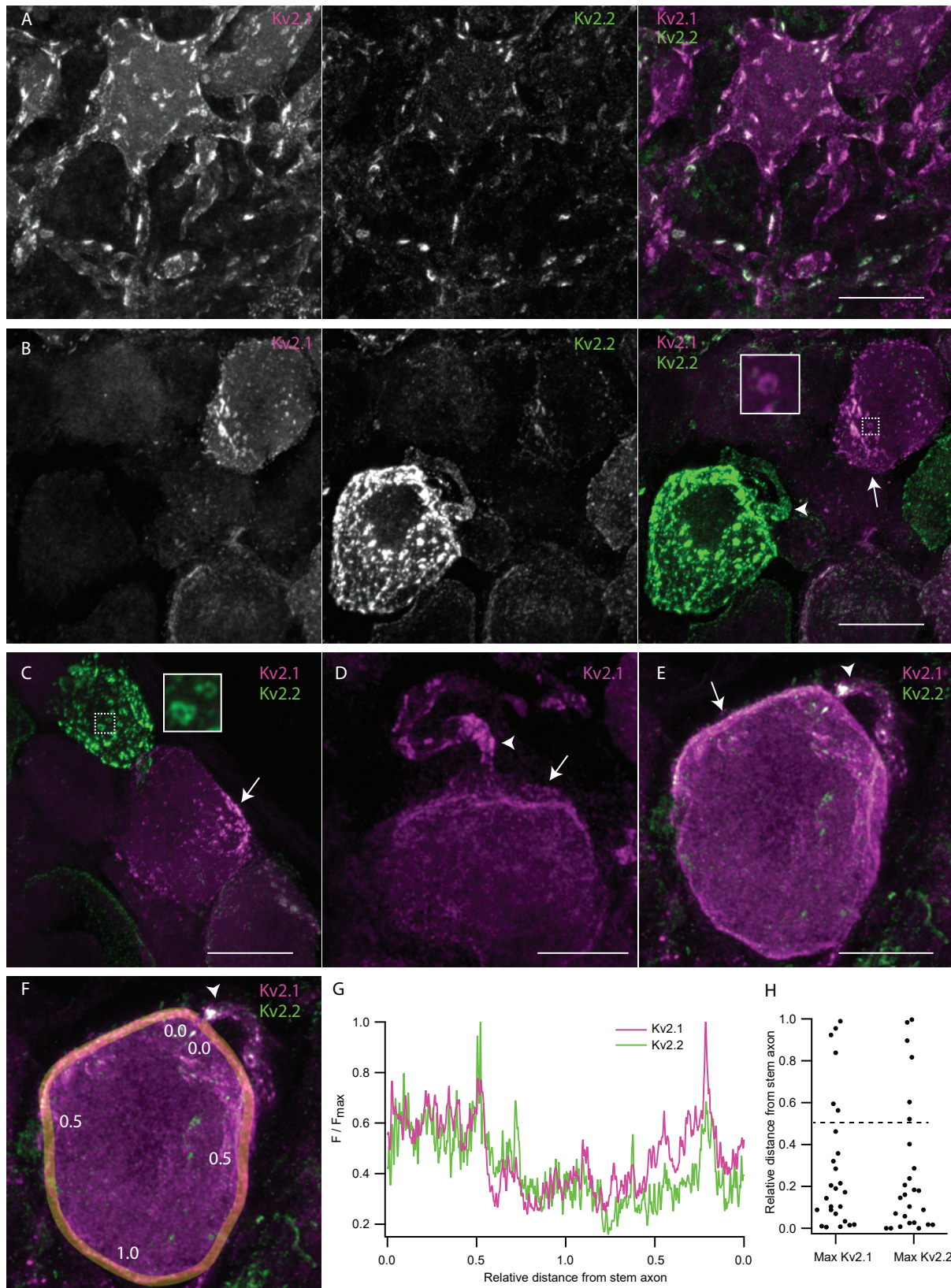
970

971 **Figure 6 legend**

972 DRG neurons have enriched Kv2.2 protein compared to neurons in the spinal cord. **A**, Anti-  
973 Kv2.1 (magenta) and anti-Kv2.2 (green) immunofluorescence in a spinal cord section from the  
974 2<sup>nd</sup> lumbar vertebra (left). Anti-Kv2.1 immunofluorescence (right top) and anti-Kv2.2  
975 immunofluorescence (right bottom). Arrows show neurons in the spinal cord with punctate  
976 anti-Kv2.1 immunofluorescence. Arrow heads show neurons in the spinal cord with anti-Kv2.2  
977 immunofluorescence. Scale bars are 500  $\mu$ m. **B**, Anti-Kv2.1 immunofluorescence from individual  
978 neuron profiles (circles) from multiple mice in the DRG and ventral horn normalized to the  
979 average fluorescence intensity of neuron profiles in the ventral horn. Diamonds to the right of  
980 data represent the average intensity of individual mice. Significant differences from 1 were  
981 calculated for individual mice using Students t-test. N = 5 mice, n = 295 in DRG and n = 200 in  
982 ventral horn. Detailed information on each mouse used can be found in table 1. **C**, Identical  
983 analysis as in panel B but with anti-Kv2.2 immunofluorescence.

984

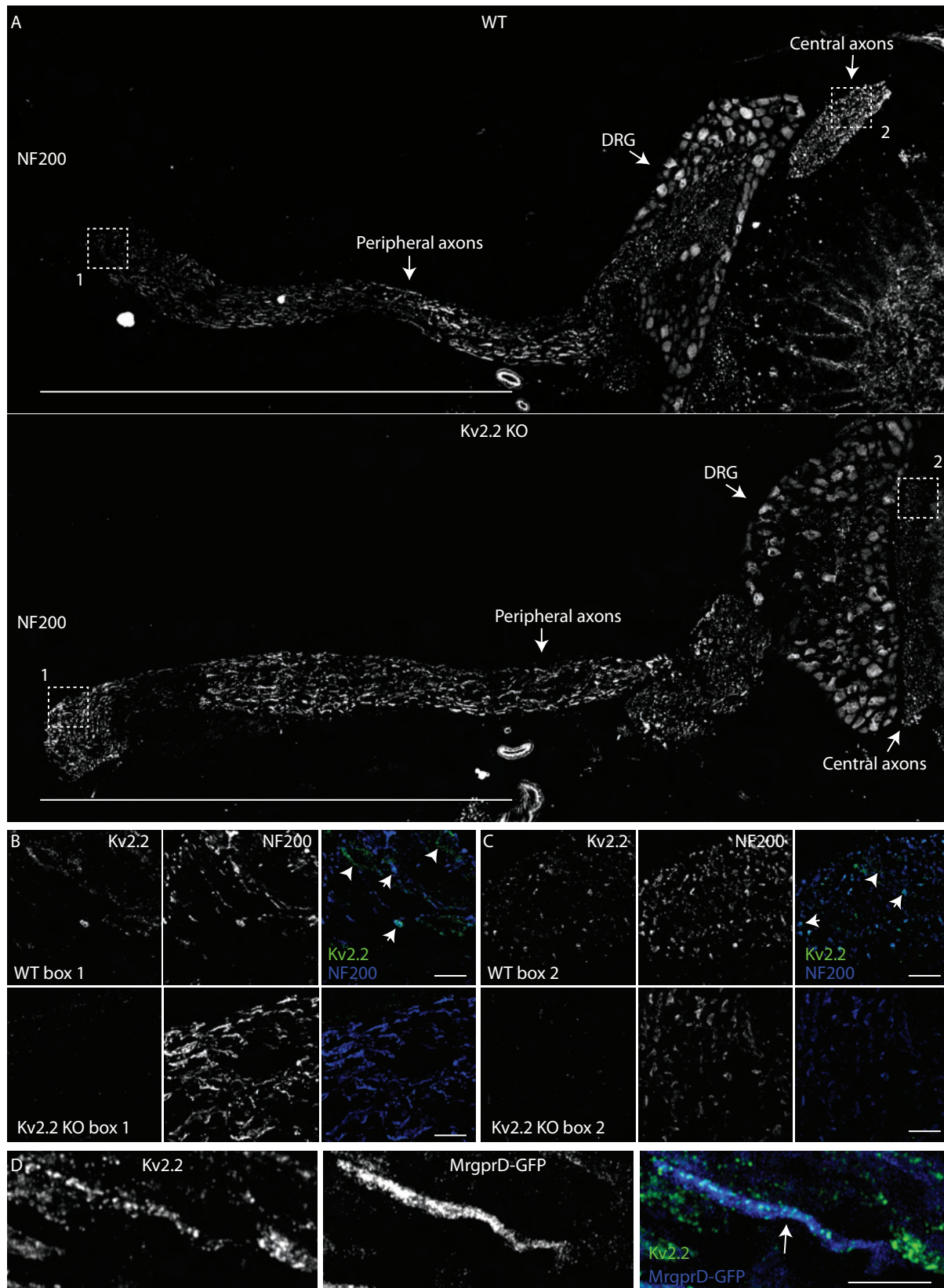
985 **Figure 7**



987 **Figure 7 legend**

988 Kv2 channels form clusters on DRG neuron somas and stem axons that are distinct from Kv2  
989 channel clusters on ventral horn neurons. **A**, Z-projection of anti-Kv2.1 and anti-Kv2.2  
990 immunofluorescence in a ventral horn neuron from the 1<sup>st</sup> lumbar vertebra of a 7 week old  
991 male mouse. **B**, Z-projection of anti-Kv2.1 and anti-Kv2.2 immunofluorescence in DRG neurons  
992 from the same mouse and section of the spinal column as neuron shown in A. Inset is  
993 enlargement of the Kv2.1 donut cluster in dotted box. **C**, Z-projection of anti-Kv2.1 and anti-  
994 Kv2.2 immunofluorescence in DRG neurons from the same mouse as A and B. Inset is  
995 enlargement of the Kv2.2 donut cluster in dotted box. **D**, Z-projection of anti-Kv2.1  
996 immunofluorescence in DRG neuron from the 13<sup>th</sup> thoracic DRG of a 24 week old male mouse.  
997 **E**, Z-projection of anti-Kv2.1 and anti-Kv2.2 immunofluorescence in DRG neuron from same  
998 mouse in D. **F**, Exemplar ROI for analyzing localization of Kv2 channel density relative to stem  
999 axon. Same image as E. ROI line width is 1.24  $\mu\text{m}$ . Numbers along line indicate approximate  
1000 distance from stem axon normalized to the midpoint of the line. **G**, Anti-Kv2.1 (magenta) and  
1001 anti-Kv2.2 (green) immunofluorescence intensity along the ROI shown in F. Distance along the  
1002 line was normalized such that the stem axon is 0 and the midpoint of the line is 1. **H**, Analysis of  
1003 the relative distance from the stem axon of the max anti-Kv2.1 or anti-Kv2.2  
1004 immunofluorescence. Dotted line represents the middle of neurons relative to the stem axon.  
1005 In all images arrows indicate asymmetrical clusters of Kv2 channels while arrow heads indicate  
1006 the apparent stem axons. Display settings are not identical between images. Scale bars are 20  
1007  $\mu\text{m}$ .  
1008

1009 **Figure 8**

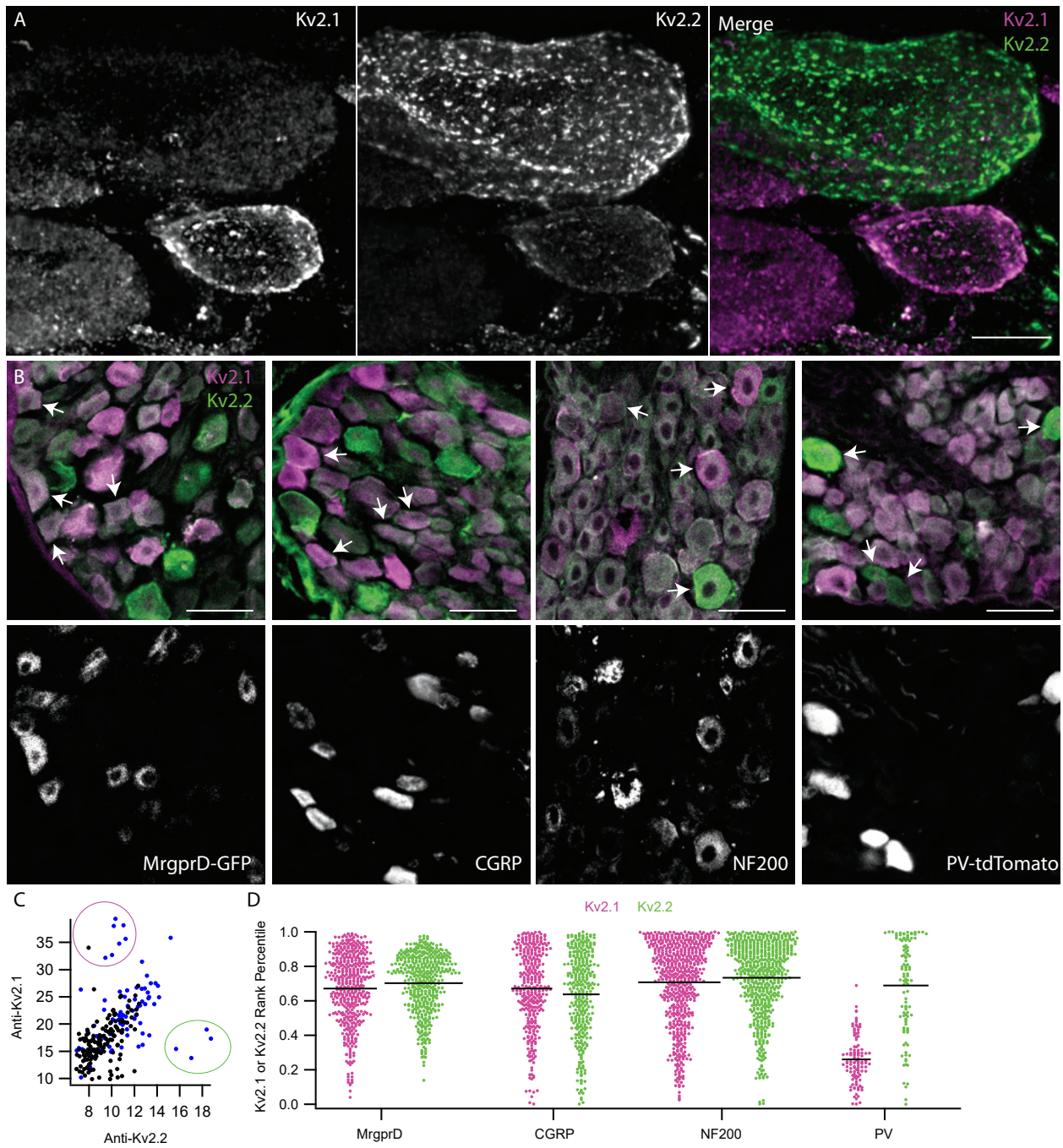


1010

1011 **Figure 8 legend**

1012 Kv2.2 channels are expressed in peripheral axons of DRG neurons. **A**, WT (top) and Kv2.2 KO  
1013 (bottom) sections containing the DRG, peripheral and central axons from the 1<sup>st</sup> lumbar DRG in  
1014 age and sex matched 7 week old mice immunolabeled for NF200 (white). Scale bar is 1 mm. **B**,  
1015 High magnification z-projection of anti-Kv2.2 and anti-NF200 immunofluorescence from box 1  
1016 in A of WT and Kv2.2 KO mice. Arrows indicate myelinated axons which show prominent anti-  
1017 Kv2.2 immunofluorescence. Scale bars are 20  $\mu\text{m}$ . **C**, High magnification z-projection of anti-  
1018 Kv2.2 and anti-NF200 immunofluorescence from box 2 in A of WT and Kv2.2 KO mice. Arrows  
1019 indicate myelinated axons which show prominent anti-Kv2.2 immunofluorescence. Scale bars  
1020 are 20  $\mu\text{m}$ . **D**, High magnification z-projection of anti-Kv2.2 immunofluorescence and MrgprD-  
1021 GFP fluorescence in the peripheral axons of the 12<sup>th</sup> thoracic DRG of a 13 week old MrgprD-GFP  
1022 mouse. Arrow indicates anti-Kv2.2 immunofluorescence on a GFP<sup>+</sup> axon. Scale bar is 10  $\mu\text{m}$ .  
1023

1024 **Figure 9**



1025

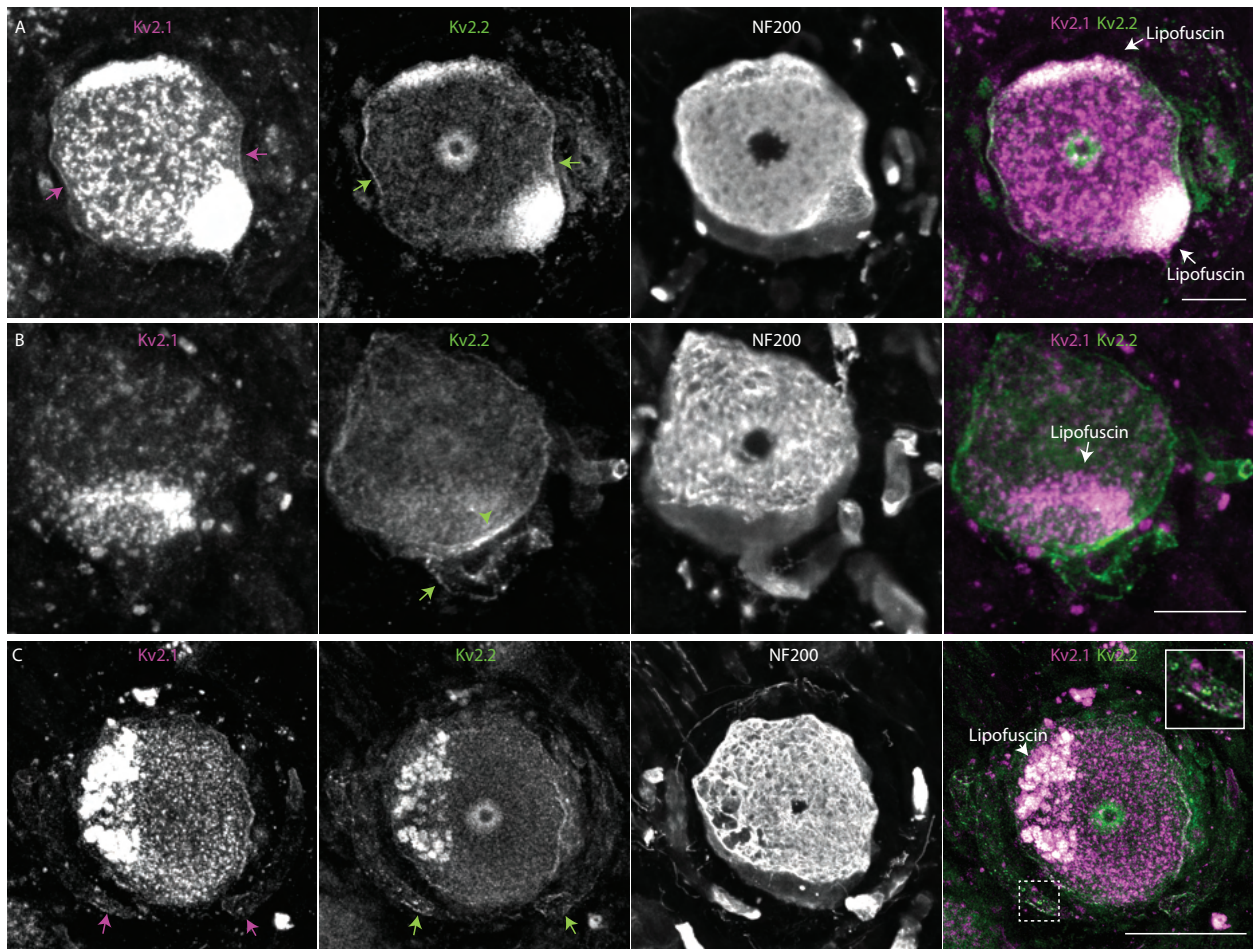
1026 **Figure 9 legend**

1027 Anti-Kv2 immunofluorescence intensities are non-uniform across DRG neuron subtypes. **A**,

1028 Exemplar z-projection of enrichment of anti-Kv2.1 (magenta) or anti-Kv2.2 (green)

1029 immunofluorescence in neighboring neurons. DRG section is from a 10 week old male mouse.  
1030 Scale bar is 10  $\mu$ m. **B**, Top images show anti-Kv2.1 (magenta) and anti-Kv2.2 (green)  
1031 immunofluorescence in DRG sections where subpopulation specific markers were used to  
1032 identify, from left to right, non-peptidergic nociceptors, peptidergic nociceptors, myelinated  
1033 neurons and proprioceptors. Fluorescence from specific markers is shown in bottom panels.  
1034 Arrows indicate four exemplar neurons that have clear positivity for each subpopulation  
1035 identified by fluorescence in lower panels. CGRP and NF200 subpopulations were identified  
1036 using anti-CGRP and anti-NF200 antibodies while MrgprD-GFP and PV-tdTomato  
1037 subpopulations were from transgenic mouse lines. Scale bars are 50  $\mu$ m. **C**, Scatter plot of anti-  
1038 Kv2.1 and anti-Kv2.2 immunofluorescence of individual neuron profiles. Each point represents  
1039 one profile. Magenta circle highlights the subpopulation of profiles that have high anti-Kv2.1  
1040 but low anti-Kv2.2 immunofluorescence while the green circle highlights the subpopulation of  
1041 profiles that have high anti-Kv2.2 but low anti-Kv2.1 immunofluorescence. Blue points  
1042 represent myelinated DRG neuron profiles identified by NF200 immunofluorescence. **D**, Ranked  
1043 anti-Kv2.1 immunofluorescence (magenta points) or ranked anti-Kv2.2 immunofluorescence  
1044 (green points) of individual profiles from subpopulations shown in B. Only profiles that were  
1045 positive for each marker are shown. Each point represents one profile. MrgprD population N = 4  
1046 mice, CGRP population N = 3 mice, NF200 population N = 3 mice and PV population N = 2 mice.  
1047 Detailed information on each mouse used can be found in table 1.  
1048

1049 **Figure 10**



1050

1051 **Figure 10 legend**

1052 Kv2 channel expression and localization in human DRG neurons is similar to mice. **A**,

1053 Immunofluorescence from human DRG neurons labeled with anti-Kv2.1 and anti-Kv2.2

1054 antibodies. Autofluorescence attributed to lipofuscin is labeled in right panel while apparent

1055 Kv2.1 and Kv2.2 protein are labeled in left and middle panel respectively. Scale bar is 50  $\mu\text{m}$ . **B**,

1056 Z-projection of anti-Kv2.2 (left) and anti-NF200 immunofluorescence (middle) of human DRG

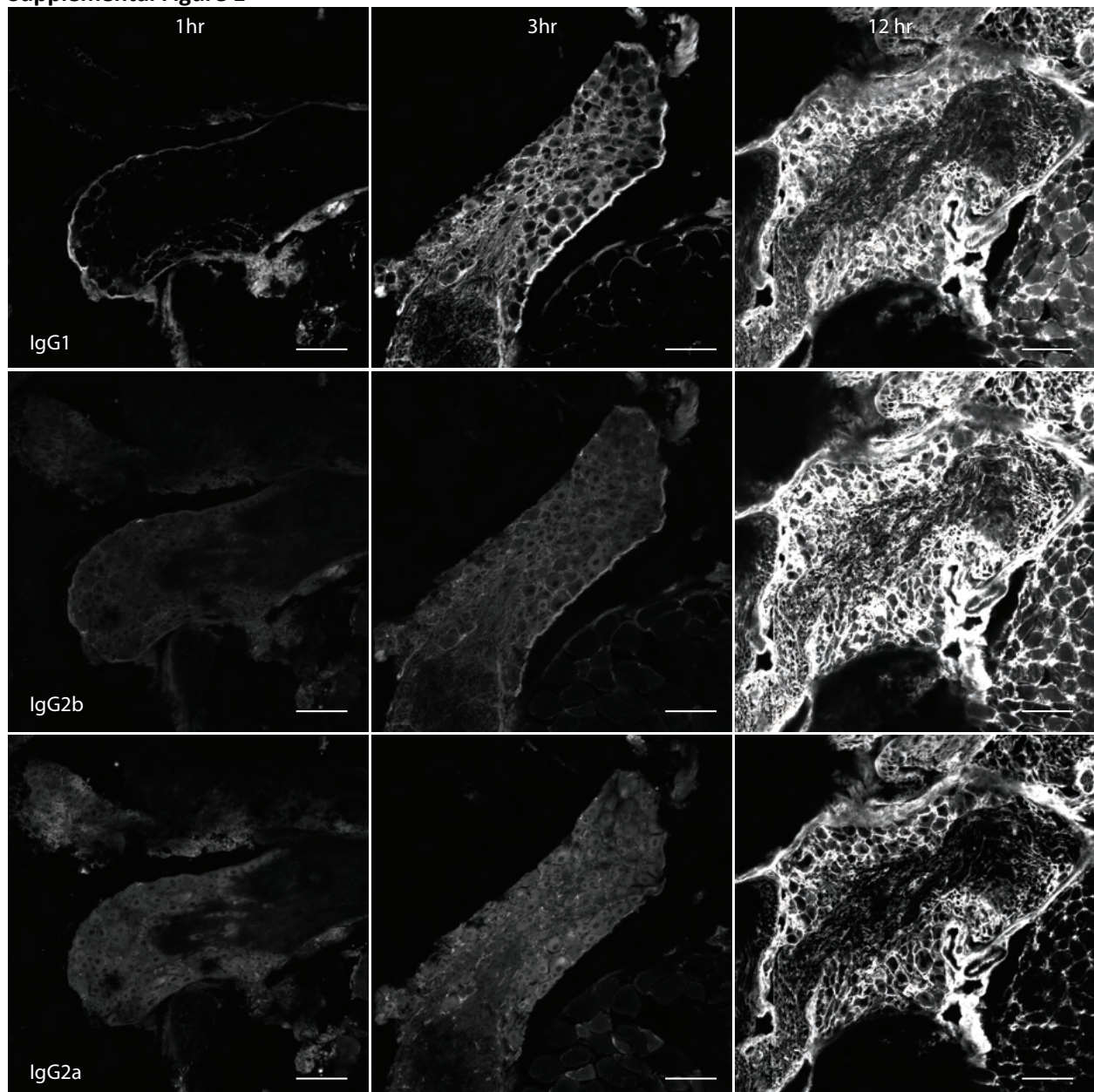
1057 neuron somata. Green arrow head indicates asymmetric distribution of Kv2.2 clusters on

1058 neuron soma, green arrow indicates the apparent stem axon. Scale bar is 20  $\mu\text{m}$ . **C**, Z-projection

1059 of anti-Kv2.1 (upper left), anti-Kv2.2 (upper right) and anti-NF200 (lower left)

1060 immunofluorescence of a human DRG neuron. Magenta and green arrows indicate Kv2.1 and  
1061 Kv2.2 respectively on the apparent stem axon. Inset shows expansion of dotted line boxes  
1062 which highlights Kv2.1 and Kv2.2 clusters on the apparent stem axon. Autofluorescence  
1063 attributed to lipofuscin is labeled in lower right panel. Scale bar is 50  $\mu\text{m}$ . All images are from  
1064 donor #1. Detailed information on each donor can be found in the *Human Tissue Collection*  
1065 section of the methods.  
1066

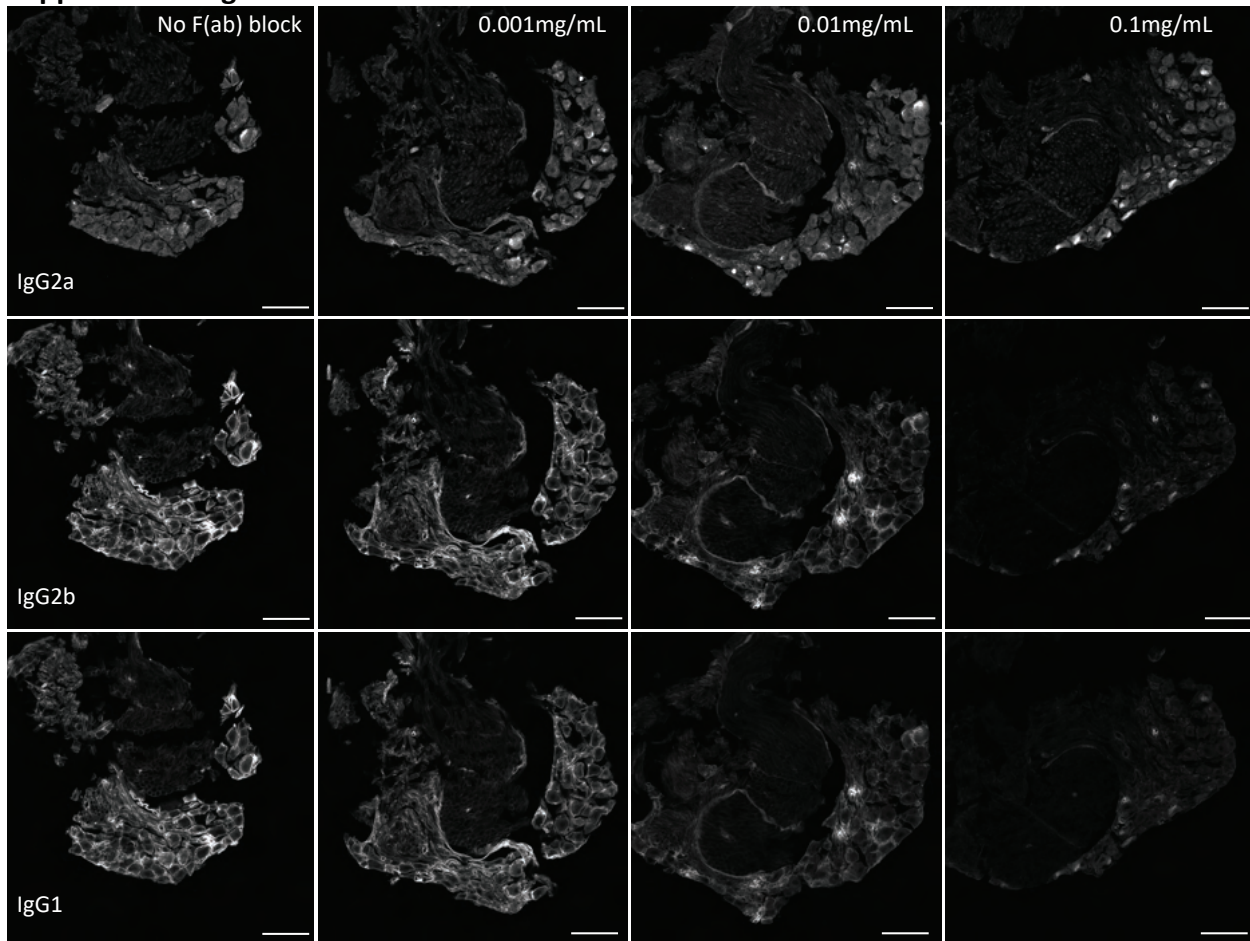
1067 **SUPPLEMENTAL FIGURES**  
1068 **Supplemental Figure 1**



1069 **Supplemental Figure 1 legend**

1070 Off-target mouse anti-IgG1, IgG2b, and IgG2a immunofluorescence increases with fixation time.  
1071 Images of DRG sections labeled with fluorescently tagged antibodies which target IgG1 (top),  
1072 IgG2b (middle) and IgG2a (bottom) after DRG were fixed in ice cold 4% PFA for 1, 3 and 12  
1073 hours. DRG sections are from the same mouse. Scale bars are 100  $\mu$ m.  
1074  
1075

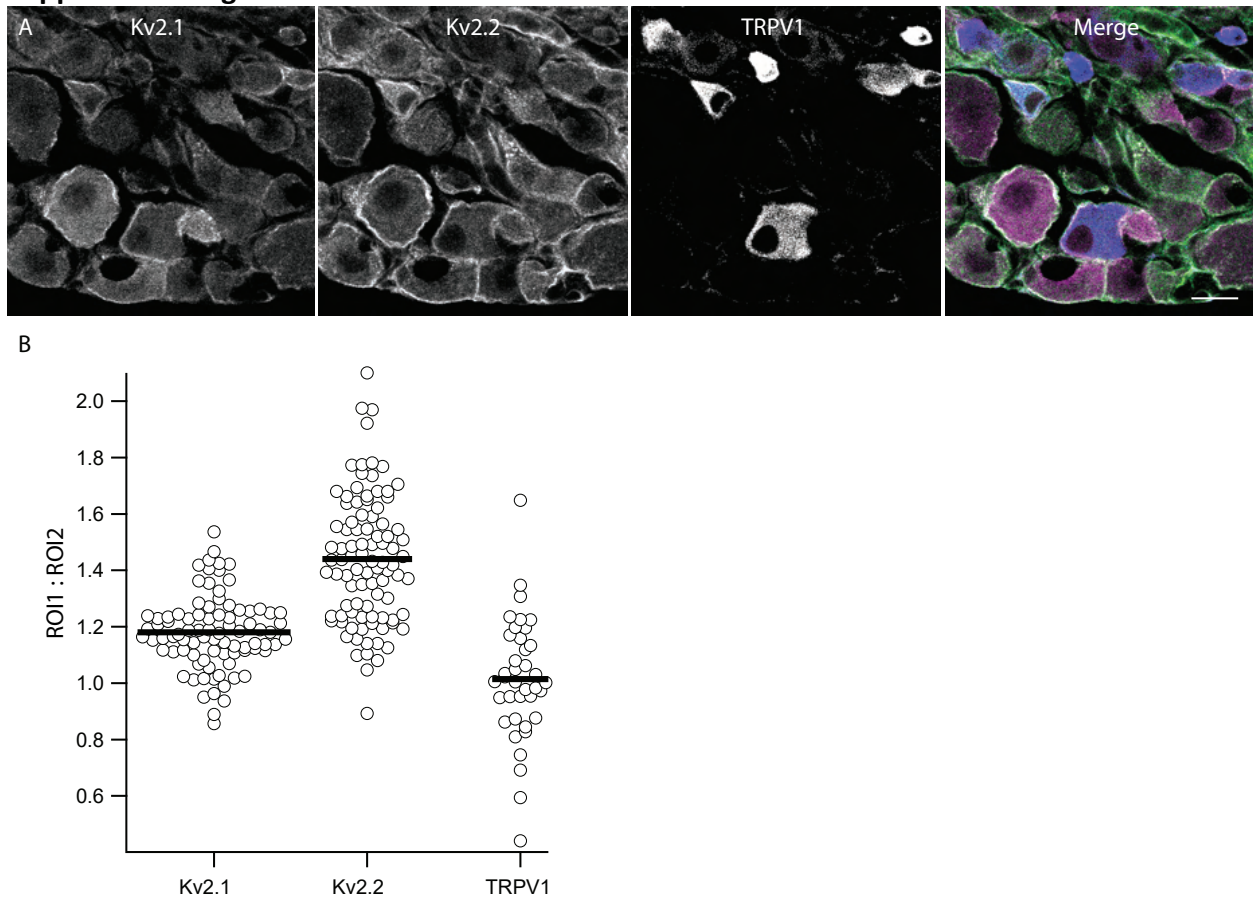
1076 **Supplemental Figure 2**



1077  
1078 **Supplemental Figure 2 legend**

1079 Pre-incubation of mouse DRG sections in IgG H+L Fab fragments reduces off target secondary  
1080 antibody labeling. Representative images of DRG sections from the same DRG treated with  
1081 increasing concentrations (left to right) of IgG H+L Fab fragment and the same concentration of  
1082 secondary antibody used in experiments throughout this study. Images were taken with  
1083 identical imaging settings and are set to the same brightness and contrast. Scale bars are 100  
1084  $\mu\text{m}$ .

1085 **Supplemental Figure 3**



1086

1087 **Supplemental Figure 3 legend**

1088 Kv2.1 and Kv2.2 protein are enriched at the outer edge of DRG neuron somas relative to TRPV1.

1089 **A**, Anti-Kv2.1, anti-Kv2.2 and anti-TRPV1 immunofluorescence from lumbar DRG neurons.

1090 Prominent cytoplasmic anti-TRPV1 immunofluorescence was observed in a subset of small

1091 diameter neurons. In merge image anti-Kv2.1, anti-Kv2.2 and anti-TRPV1 immunofluorescence

1092 are magenta, green and blue respectively. Scale bar is 20  $\mu$ m. **B**, Ratio of average anti-Kv2.1,

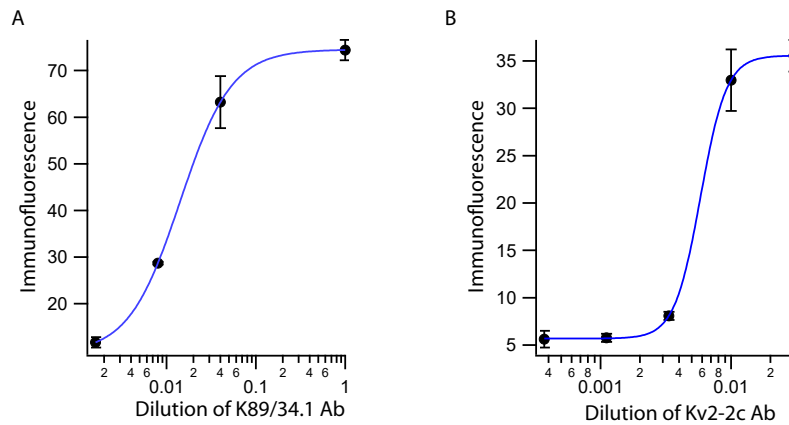
1093 anti-Kv2.2 or anti-TRPV1 immunofluorescence from outer and inner ROIs for individual

1094 neurons.

1095

1096

1097 **Supplemental Figure 4**

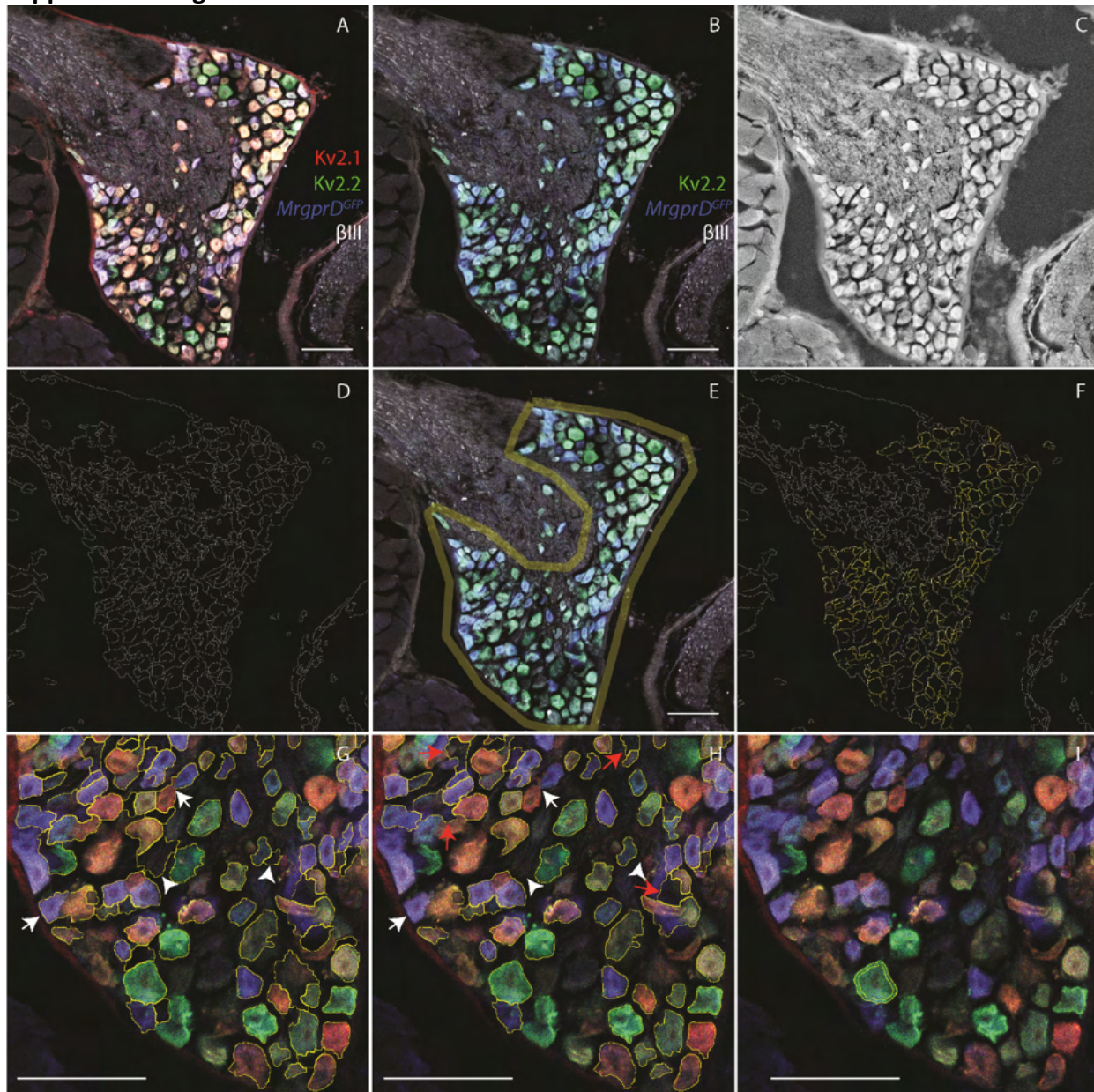


1098

1099 **Supplemental Figure 4 legend**

1100 Kv2 antibodies used in knockout experiments are at saturating concentrations. **A**,  
1101 Concentration response of immunofluorescence from sections labeled with anti-Kv2.1 antibody  
1102 used in Figure 2. Blue line is a Hill fit of the data. 1:1 = 2 sections, 1:25 = 3 sections, 1:125 = 2  
1103 sections, 1:625 = 3 sections **B**, Concentration response of immunofluorescence from sections  
1104 labeled with anti-Kv2.2 antibody used in Figure 3. Blue line is a Hill fit of the data. 1:33 = 2  
1105 sections, 1:100 = 10 sections, 1:300 = 4 sections, 1:900 = 4 sections, 1:2700 = 3 sections  
1106

1107 **Supplemental Figure 5**



1108

1109

**Supplemental Figure 5 legend**

1110 A method to sample neurons in DRG imaging data using watershed segmentation identifies the

1111 outer region of neurons. **A**, Image of anti-Kv2.1, anti-Kv2.2, anti- $\beta$ III tubulin

1112 immunofluorescence and MrgprD-GFP fluorescence. **B**, Same image as **A** with anti-Kv2.1

1113 immunofluorescence channel removed as this is an example of processing data for Kv2.1 KO

1114 analysis. **C**, Grayscale image of average fluorescence from all three channels shown in **B**.

1115 Gaussian and median filters were applied to image to improve watershed segmentation. **D**,

1116 Watershed segmentation of image in **C** using the MorphoLibJ Morphological Segmentation

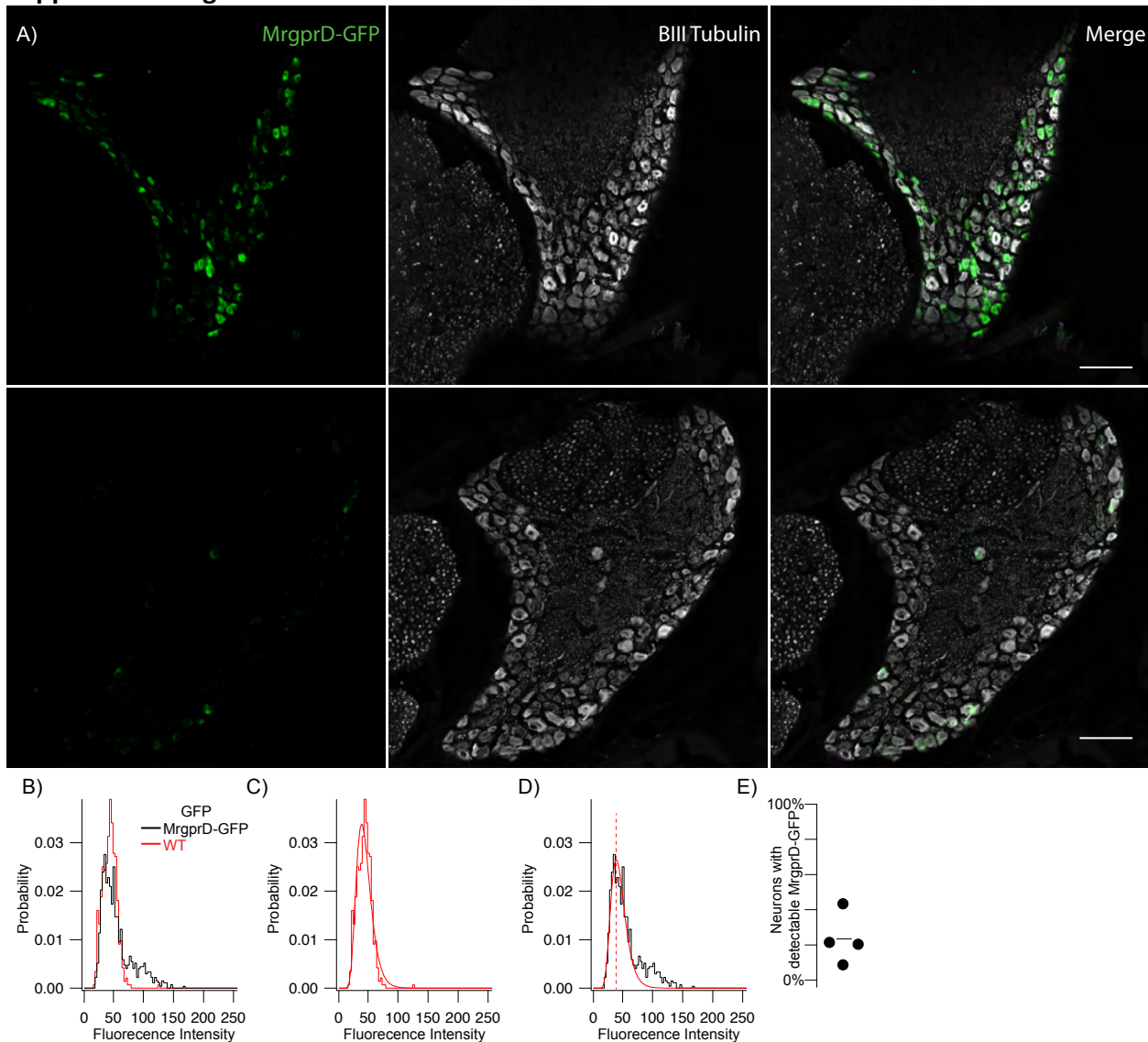
1117 Plugin in Fiji. **E**, Example of manually drawn boundary that encompasses the neuron somas in

1118 the DRG so that only these watershed lines are selected. **F**, Selected ROIs from watershed

1119 segmentation (yellow). ROIs were excluded based on roundness and size using the Analyze

1120 Particles tool in Fiji. **G**, ROIs in F overlaid on DRG image showing that some ROIs are selecting  
1121 regions that do not contain neurons (arrow heads) or are selecting multiple neurons (arrows).  
1122 **H**, ROIs after processing using an in-house R script which removes ROIs that do not contain  
1123 neurons (arrow heads) and ROIs that contain two neurons (arrows). This script did not remove  
1124 all ROIs that do not contain neurons (red arrows). Each experiment performed was done  
1125 alongside controls where the primary antibodies were omitted and fluorescence from these  
1126 control sections was used by the in-house R script to identify and remove ROIs that do not  
1127 contain neurons. **I**, Example of automatically generated annulus that encompasses the outer  
1128 edge of the soma. Scale bars are 100  $\mu\text{m}$ .  
1129

1130 **Supplemental Figure 6**



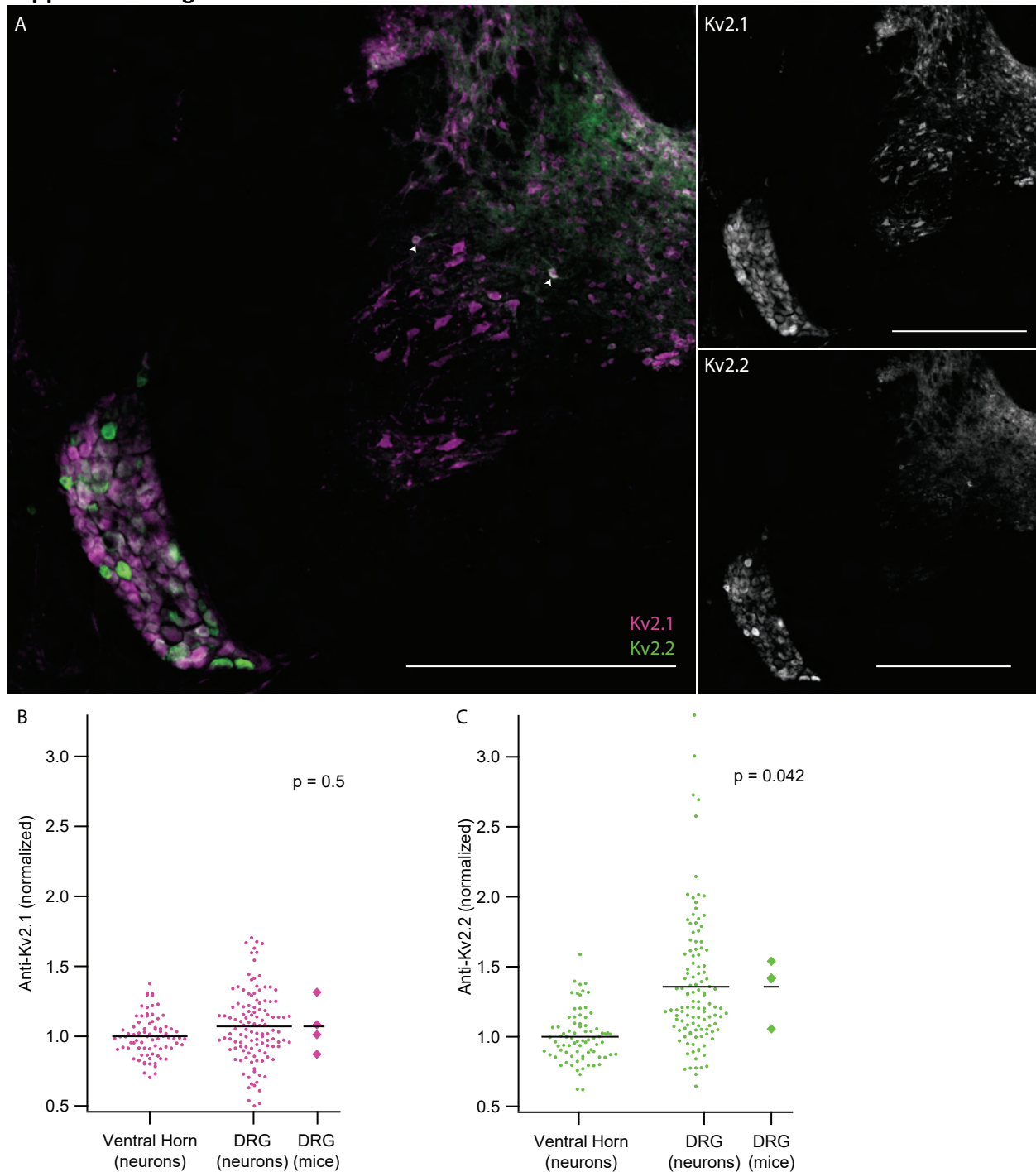
1131

1132

**Supplemental Figure 6 legend**

1133 Method used to estimate percent of neurons expressing Kv2.1 and Kv2.2 reliably predicts the  
1134 percentage of neurons that express GFP in MrgprD-GFP mice. **A**, MrgprD-GFP (top) and WT  
1135 (bottom) DRG sections immunolabeled for BIII tubulin (white). Images were taken with identical  
1136 imaging settings and are set to the same brightness and contrast. Scale bars are 100 μm. **B**,  
1137 Distribution of fluorescence intensity from MrgprD-GFP (black) and WT (red) neurons. Data  
1138 represents the fluorescence intensity of 905 MrgprD-GFP neurons from 9 DRG sections from 1  
1139 mouse or 477 WT neurons from 5 DRG sections from 1 mouse. DRG sections were taken from 7  
1140 week old female mice and are from the 1<sup>st</sup> lumbar DRG. **C**, WT data shown in B fit with a log  
1141 normal distribution (red fit). **D**, MrgprD-GFP data shown in B fit with the WT distribution (red  
1142 fit) where width and mean were constrained to the WT distribution and amplitude was  
1143 unconstrained (equation 1). Only MrgprD-GFP data to the left of the mean intensity of WT  
1144 neurons (red dotted line) was used for the fit. **E**, Percent of neurons with detectable GFP  
1145 protein of 4 mice (3 females 1 male). All DRG sections were taken from the 1<sup>st</sup> lumbar DRG.

1146 **Supplemental Figure 7**



1147

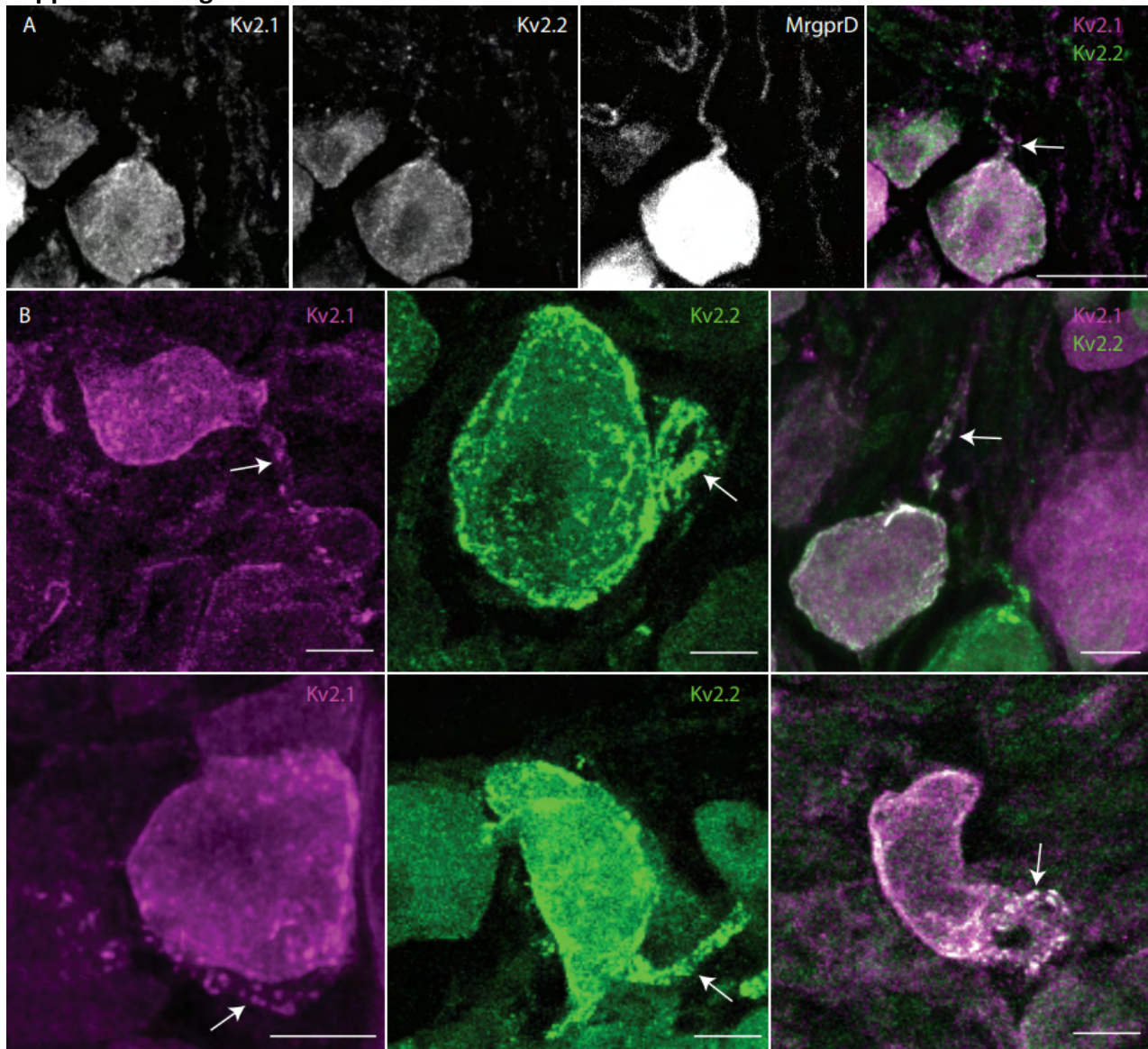
1148

**Supplemental Figure 7 legend**

1149 DRG neurons have enriched Kv2.2 protein compared to neurons in the ventral horn. **A**, Anti-  
1150 Kv2.1 (magenta) and anti-Kv2.2 (green) immunofluorescence in a spinal cord section from the  
1151 13<sup>th</sup> thoracic vertebra (left). Anti-Kv2.1 immunofluorescence (right top) and anti-Kv2.2  
1152 immunofluorescence (right bottom). Arrow heads show neurons in the spinal cord with anti-  
1153 Kv2.2 immunofluorescence. Scale bars are 500  $\mu$ m. **B**, Anti-Kv2.1 immunofluorescence from

1154 individual neurons (circles) in the DRG and ventral horn normalized to the average fluorescence  
1155 intensity of neurons in the ventral horn. Diamonds to the right of data represent the average  
1156 intensity in the DRG of individual mice. Significant differences from 1 were calculated for  
1157 individual mice using Students t-test. N = 4 mice n = 116 in DRG and n = 77 in ventral horn. **C**,  
1158 Identical analysis shown in B with anti-Kv2.2 immunofluorescence.  
1159

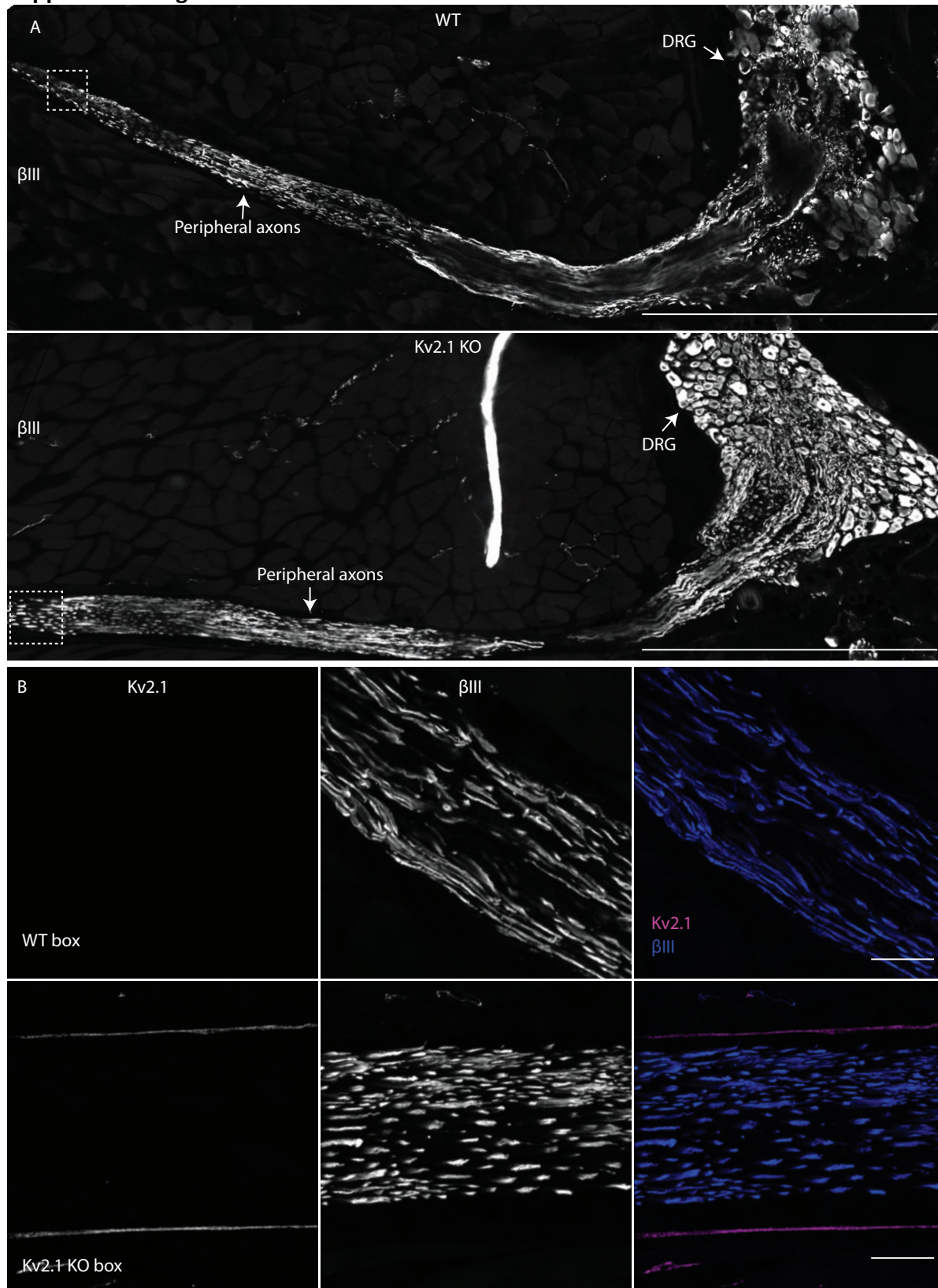
1160 **Supplemental Figure 8**



1161  
1162 **Supplemental Figure 8 legend**

1163 Kv2 channels are expressed on the stem axon of mouse DRG neurons. **A**, Z-projection with anti-  
1164 Kv2.1 and anti-Kv2.2 immunofluorescence on the stem axon of a neuron in the DRG of a  
1165 MrgprD-GFP mouse. **B**, Gallery of z-projected images of DRG neurons with anti-Kv2.1 and/or  
1166 anti-Kv2.2 immunofluorescence on stem axons. Arrows indicate stem axons. Scale bars are 10  
1167  $\mu\text{m}$

1168 **Supplemental Figure 9**



1169

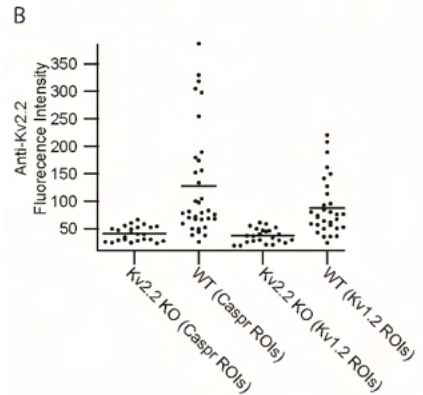
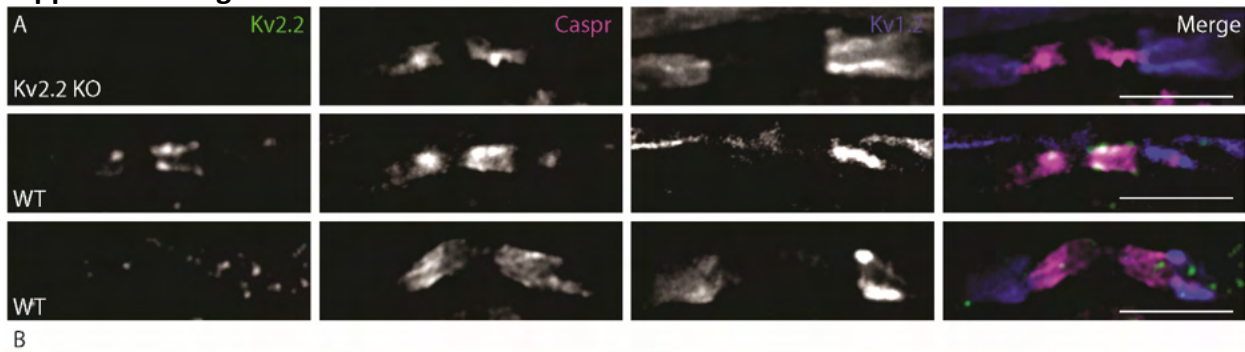
1170 **Supplemental Figure 9 legend**

1171 Kv2.1 channels were not detected in peripheral axons of DRG neurons. **A**, WT (top) and Kv2.1  
1172 KO (bottom) sections containing the DRG and peripheral axons from the 12<sup>th</sup> thoracic DRG in  
1173 age and sex matched 7 week old mice immunolabeled for  $\beta$ III tubulin (white). Scale bar is 500  
1174  $\mu$ m. **B**, High magnification z-projection of anti-Kv2.1 and anti- $\beta$ III immunofluorescence from box  
1175 in A of WT and Kv2.1 KO mice. Scale bars are 20  $\mu$ m.

1176

1177

1178 **Supplemental Figure 10**



1179

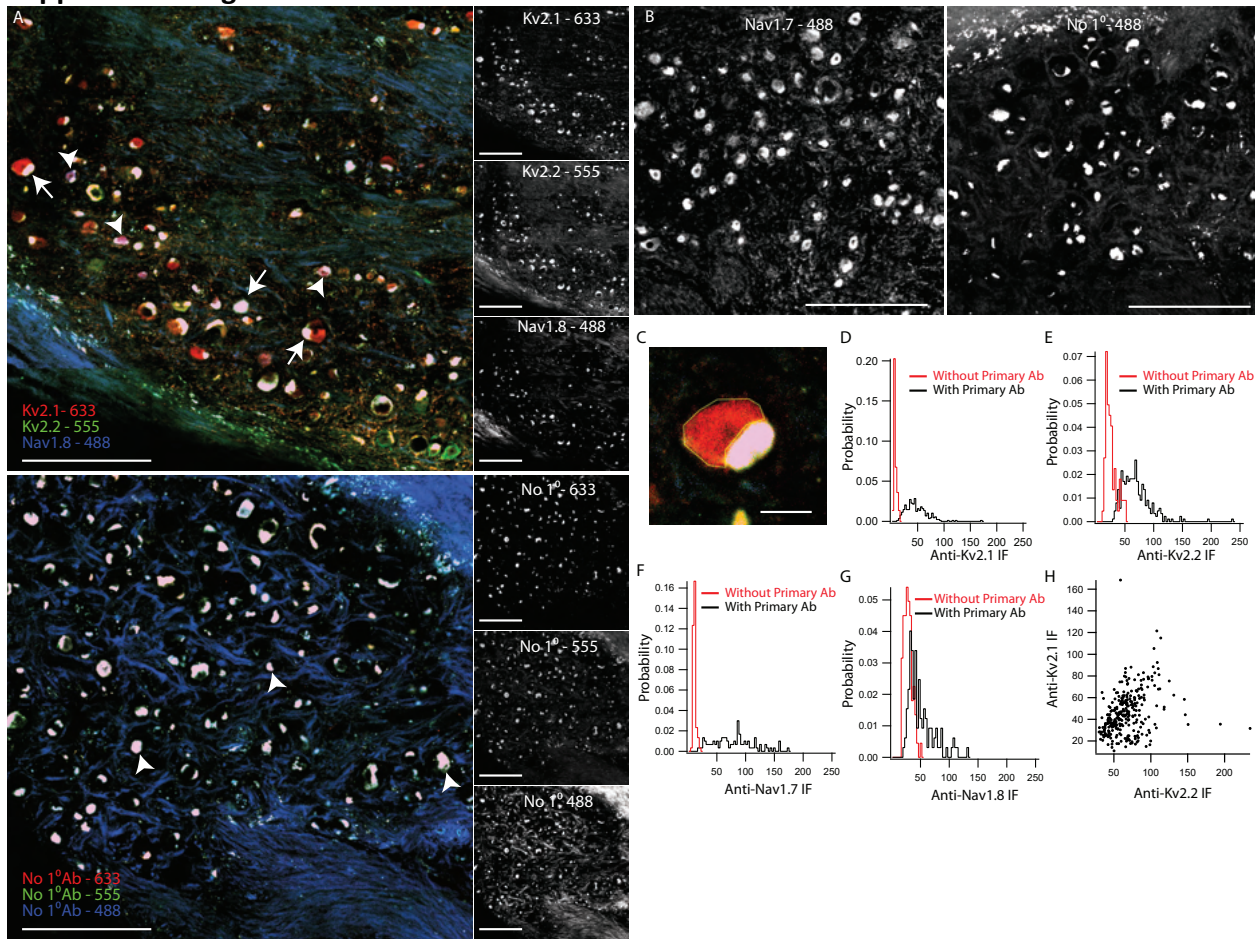
1180 **Supplemental Figure 10 legend**

1181 Kv2.2 is expressed in myelinated fibers of DRG neuron axons. **A**, Kv2.2 KO (top) and WT (middle  
1182 and bottom) sections containing the peripheral axons from the 12<sup>th</sup> thoracic DRG in 28 week  
1183 old mice immunolabeled for Kv2.2, Caspr and Kv1.2. Middle panels are an exemplar of  
1184 prominent Kv2.2 immunofluorescence in CASPR labeled axons and bottom panels are an  
1185 exemplar of prominent Kv2.2 clusters in the Kv1.2 labeled axons. Scale bars are 5  $\mu$ m. **B**,  
1186 Analysis of anti-Kv2.2 immunofluorescence intensity in CASPR and Kv1.2 labeled regions of age  
1187 and sex matched WT and Kv2.2 KO mice. Individual points represent single ROIs drawn around  
1188 anti-CASPR or anti-Kv1.2 immunofluorescence.

1189

1190

1191 **Supplemental Figure 11**

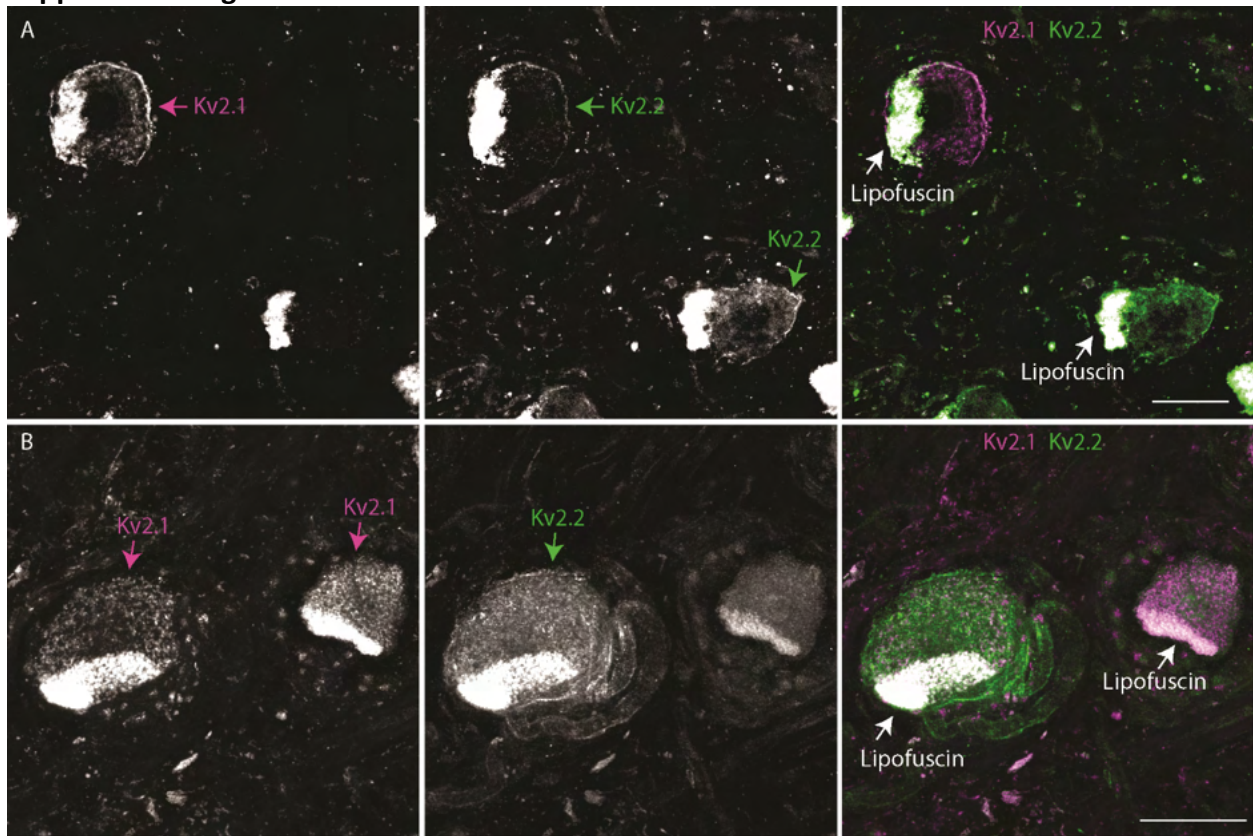


1192  
1193 **Supplemental Figure 11 legend**

1194 Fluorescence from human DRG neurons labeled with ion channel targeting antibodies is distinct  
1195 from human DRG neurons where ion channel targeting antibodies were omitted. **A**, Top:  
1196 Immunofluorescence from human DRG section labeled with anti-Kv2.1, anti-Kv2.2 and anti-  
1197 Nav1.8 antibodies. Bottom: Fluorescence from human DRG section where the primary  
1198 antibodies are omitted. Arrows in top and bottom images indicate examples of  
1199 autofluorescence from apparent intracellular lipofuscin. Arrow heads in top image identify anti-  
1200 Nav1.8 immunofluorescence. Images on the right are fluorescence from each fluorescence  
1201 channel of the top and bottom images. Number next to target protein label represents  
1202 excitation wavelength. DRG sections from top and bottom images are from the same DRG.  
1203 Scale bars are 500  $\mu$ m. **B**, Left: Immunofluorescence from human DRG section labeled with anti-  
1204 Nav1.7 antibody. Right: Fluorescence from human DRG section where the primary antibody has  
1205 been omitted. Number next to target protein label represents excitation wavelength. DRG  
1206 sections in left and right images are from the same DRG. Scale bars are 500  $\mu$ m. **C**, Exemplar  
1207 manually drawn ROI to analyze fluorescence intensity in human DRG neurons that omits  
1208 apparent lipofuscin autofluorescence. Scale bar is 50  $\mu$ m. **D**, Distribution of fluorescence  
1209 intensity of human DRG neurons labeled with an anti-Kv2.1 antibody (black) or when the anti-  
1210 Kv2.1 antibody was omitted (red). Data represents the fluorescence intensity of 293 neurons  
1211 labeled with anti-Kv2.1 antibody or 73 neurons where the anti-Kv2.1 antibody was omitted. **E**,

1212 Distribution of fluorescence intensity of human DRG neurons labeled with anti-Kv2.2 antibody  
1213 (black) or when the anti-Kv2.2 antibody was omitted (red). Data represents the fluorescence  
1214 intensity of 293 neurons labeled with anti-Kv2.2 antibody or 73 neurons where the anti-Kv2.2  
1215 antibody was omitted. **F**, Distribution of fluorescence intensity of human DRG neurons labeled  
1216 with anti-Nav1.7 antibody (black) or when the anti-Nav1.7 antibody was omitted (red). Data  
1217 represents the fluorescence intensity of 99 neurons labeled with anti-Nav1.7 antibody or 99  
1218 neurons where the anti-Nav1.7 antibody was omitted. **G**, Distribution of fluorescence intensity  
1219 of human DRG neurons labeled with anti-Nav1.8 antibody (black) or when the anti-Nav1.8  
1220 antibody was omitted (red). Data represents the fluorescence intensity of 293 neurons labeled  
1221 with anti-Nav1.8 antibody or 73 neurons where the anti-Nav1.8 antibody was omitted. **H**,  
1222 Fluorescence intensity of human neurons labeled with both anti-Kv2.1 and anti-Kv2.2  
1223 antibodies. Individual points represent individual neurons. All images are from donor #2.  
1224 Detailed information on each donor can be found in the *Human Tissue Collection* section of the  
1225 methods.  
1226

1227 **Supplemental Figure 12**

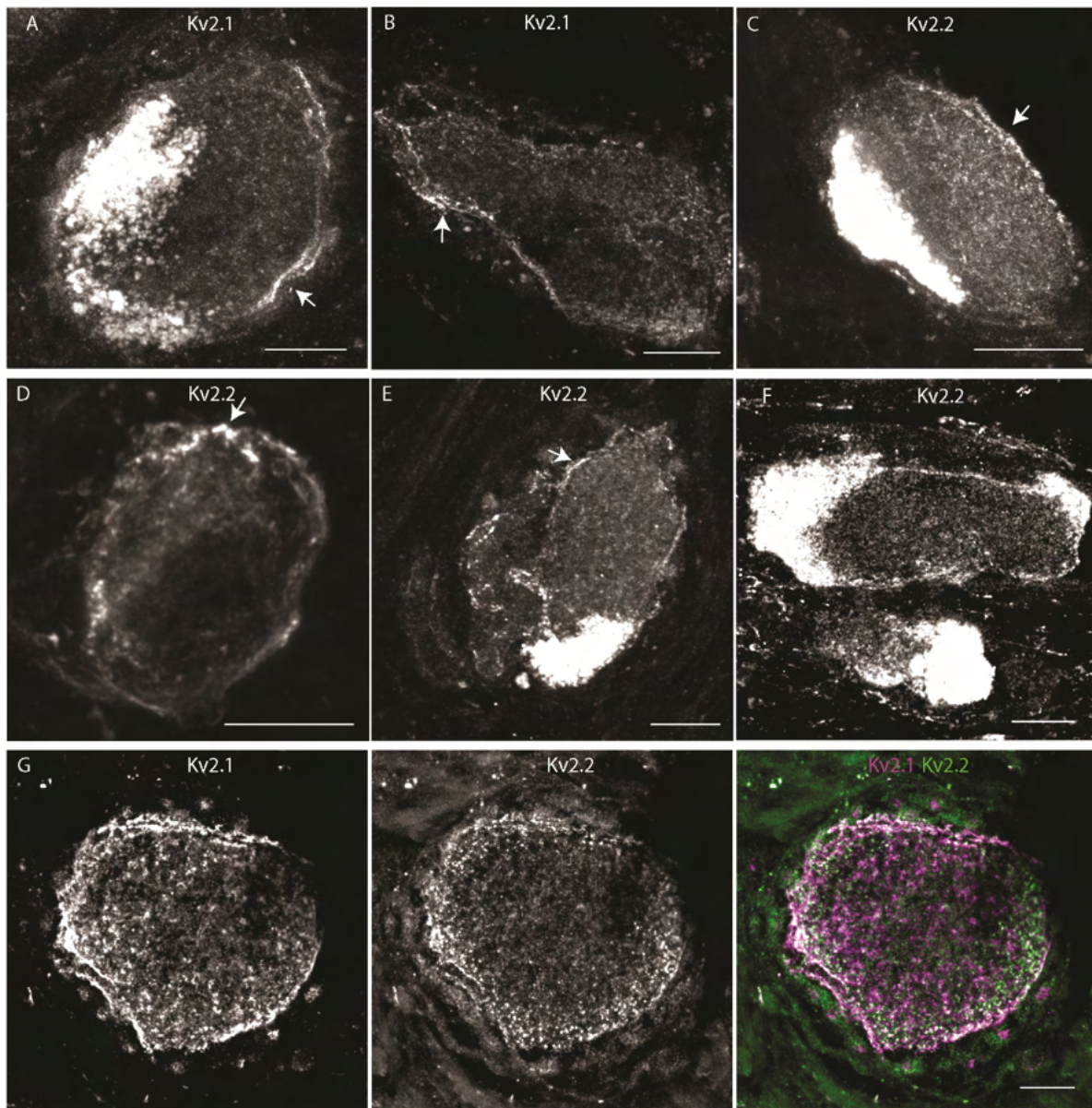


1228  
1229 **Supplemental Figure 12 legend**

1230 Immunofluorescence from human DRG neurons from donor #2 **A** and donor #3 **B** labeled with  
1231 anti-Kv2.1 and anti-Kv2.2 antibodies. Autofluorescence attributed to lipofuscin is labeled in  
1232 right panels while apparent Kv2.1 and Kv2.2 protein are labeled in left and middle panels  
1233 respectively. Scale bars are 50  $\mu$ m. Detailed information on each donor can be found in the  
1234 *Human Tissue Collection* section of the methods.

1235

1236 **Supplemental Figure 13**

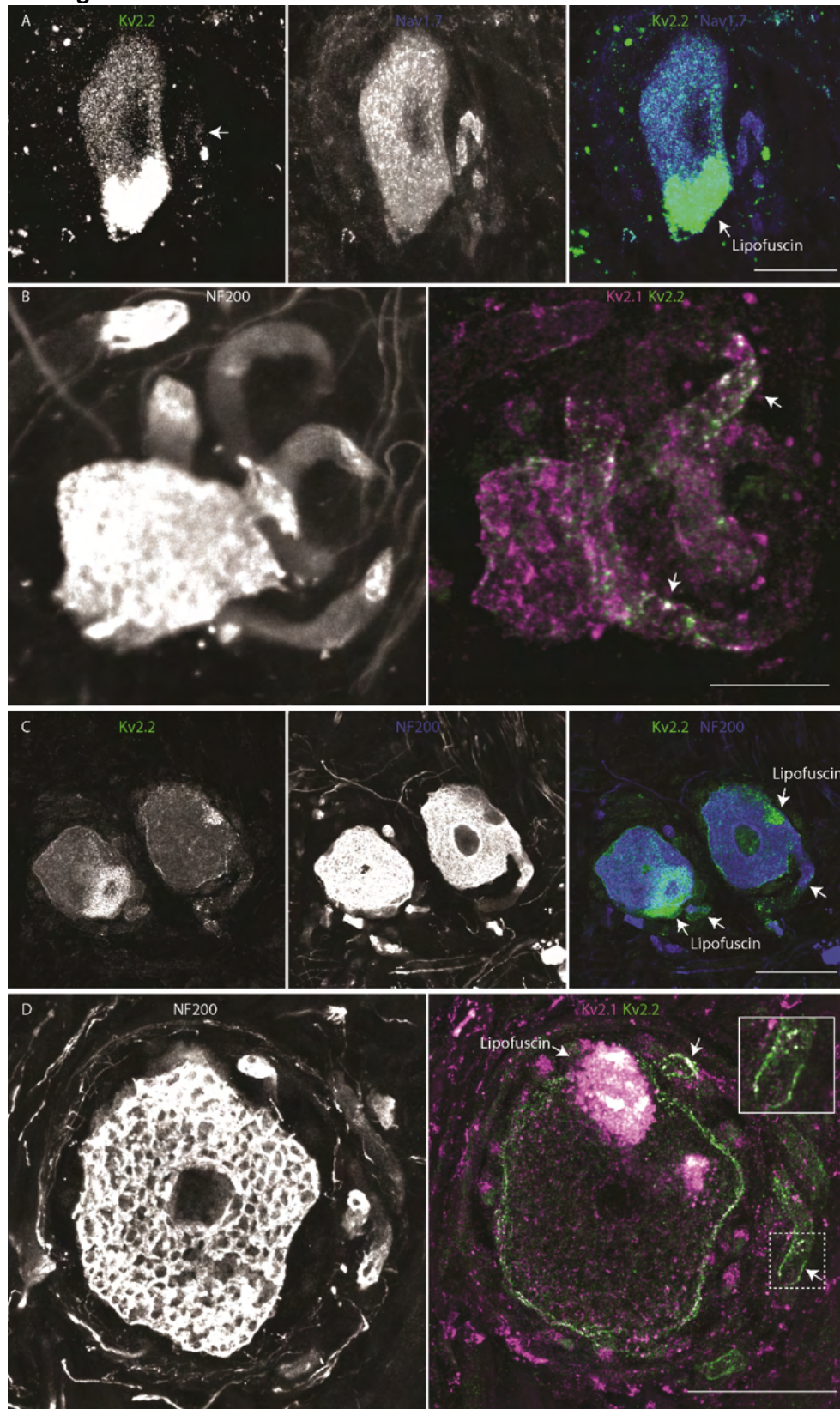


1237  
1238 **Supplemental Figure 13 legend**

1239 Kv2 channels are enriched at the outer edge of human DRG neurons. **A-B**, Exemplar z-  
1240 projections of anti-Kv2.1 immunofluorescence enriched at the outer surface of human DRG  
1241 neurons. Arrows indicate asymmetric clusters. Images are from donor #2. Scale bars are 20 μm.  
1242 **C-F**, Exemplar z-projections of anti-Kv2.2 immunofluorescence enriched at the outer surface of  
1243 a human DRG neurons. Arrows indicate asymmetric clusters. Image in **E** is from donor #3 while  
1244 all other images are from donor #2. Scale bars are 20 μm. **G**, Exemplar z-projection of anti-Kv2.1  
1245 and anti-Kv2.2 immunofluorescence both enriched at the outer surface of a human DRG neuron  
1246 soma. Image is from donor #2. Scale bar is 20 μm. Detailed information on each donor can be  
1247 found in the *Human Tissue Collection* section of the methods.

1248

1249 Supplemental Figure 14



1250  
1251

1252 **Supplemental Figure 14 legend**

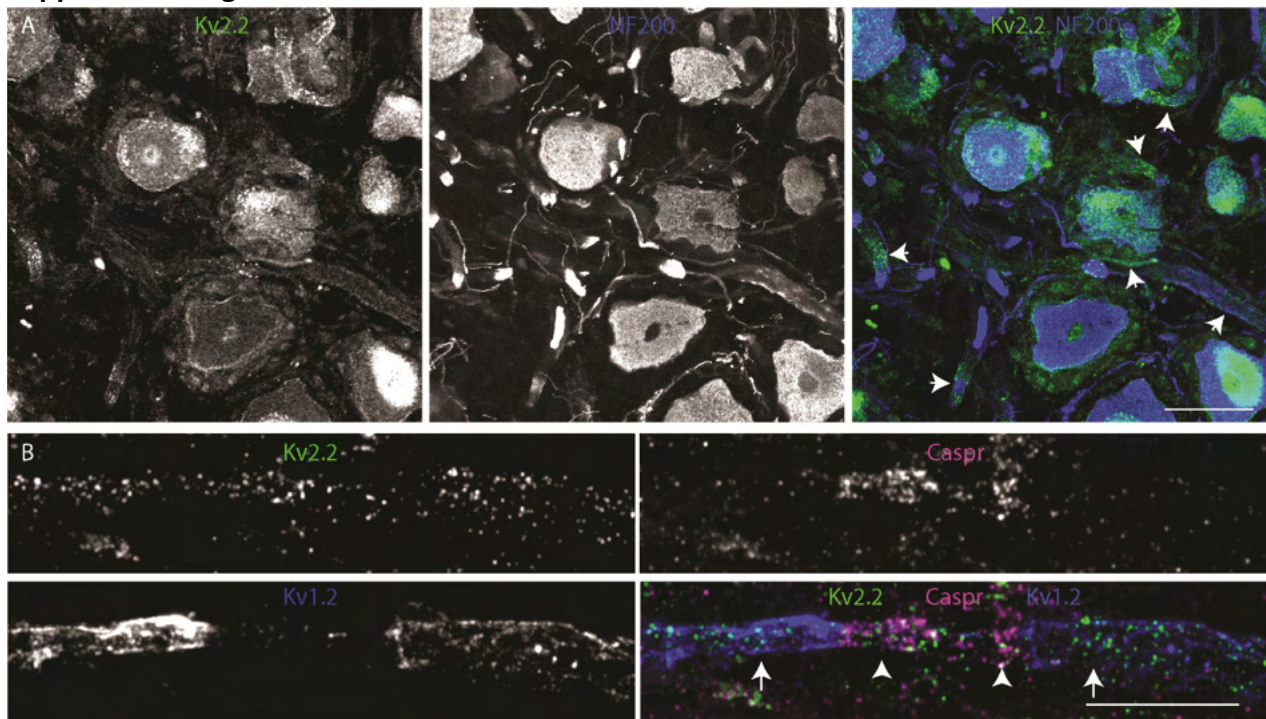
1253 **A**, Z-projection of anti-Kv2.2 and anti-Nav1.7 immunofluorescence in a human DRG neuron  
1254 soma and stem axon. Arrow in merge indicates the stem axon of the DRG neuron. Apparent  
1255 lipofuscin autofluorescence is labeled in merge. Image is from donor #2. Scale bar is 20  $\mu\text{m}$ . **B**,  
1256 Z-projection of anti-Kv2.1 (magenta), anti-Kv2.2 (green) (right) and anti-NF200 (left)  
1257 immunofluorescence in a human DRG neuron soma and stem axon. Arrows in merge indicate  
1258 the stem axon of the DRG neuron. Image is from donor #1. Scale bar is 20  $\mu\text{m}$ . **C**, Z-projection of  
1259 anti-Kv2.2 (left) and anti-NF200 (middle) immunofluorescence in a human DRG neuron soma  
1260 and stem axon. Arrow in merge indicates the stem axon of the DRG neuron. Apparent lipofuscin  
1261 autofluorescence is labeled in merge. Image is from donor #1. Scale bar is 50  $\mu\text{m}$ . **D**, Z-  
1262 projection of anti-Kv2.1 (magenta), anti-Kv2.2 (green) (right) and anti-NF200 (left)  
1263 immunofluorescence in a human DRG neuron soma and stem axon. Arrows in merge indicate  
1264 the stem axon of the DRG neuron. Apparent lipofuscin autofluorescence is labeled in merge.  
1265 Image is from donor #3. Scale bar is 50  $\mu\text{m}$ . Detailed information on each donor can be found in  
1266 the *Human Tissue Collection* section of the methods.

1267

1268

1269

1270 **Supplemental Figure 15**



1271

1272 **Supplemental Figure 15 legend**

1273 **A**, Z-projection of anti-Kv2.2 (left) and anti-NF200 (middle) immunofluorescence of human DRG.

1274 Arrows in merge represent exemplar axons which have clear anti-Kv2.2 immunofluorescence.

1275 Image is from donor #1. Scale bar is 50 μm. **B**, Z-projection of anti-Kv2.2 (upper left), anti-CASPR

1276 (upper right) and anti-Kv1.2 (bottom left) immunofluorescence of human DRG axon. Image is

1277 from donor #2. Scale bar is 10 μm. Detailed information on each donor can be found in the

1278 *Human Tissue Collection* section of the methods.

1279

1280

1281 **TABLE 1**

Figure	Genotype	Number of Mice (N)	Sections/plates Analyzed	ROIs Analyzed (n)	Age (Weeks)	Sex	Level of spinal column	Total ROIs analyzed
1	WT	1	1	124	11	M	L	124
2	WT	5	3,4,10,8,4	52,172,476,437,134,	16,7,7,7,7	M,M,F, M,M	L,T12,T12,T12, T12	1271
	Kv2.1 KO	5	4,7,5,4,5	232,124,576,293,239,	16,7,7,7,7	M,M,F, M,M	L,T12,T12,T12, T12	1124
3	WT	8	4,11,4,6,4,4,4,6	238,126,1227,673,706,748,602,572,	50,50,50,7,7,24,7,28	M,M,M, M,M, M,M,F	L,T12,T12,T12, T12,T12,L1, T12	4892
	Kv2.2 KO	8	3,6,7,4,4,4,4,5	359,209,853,400,913,719,729,745,	50,50,50,7,7,24,7,28	M,M,M, M,M, M,M,F	L,T12,T12,T12, T12,T12,L1, T12	4927
4	WT	10	7,5,6,9,8	444,268,167,669,600,	50,50,50,50,50	F,F,F,M, M	T12,T12,T12,T12,T12	3419
	Kv2.1 KO	7	5,6	298,324,	50,50	M,M	T12,T12	622
	WT	8	same as data in figure 3					
	Kv2.2 KO	8	same as data in figure 3					
5	WT	3	4,16,17,	104,379,328,	18,19,19	F,F,F	L,L,L	811
	Kv2.1 Kv2.2 DKO	2	5,14,	108,274,	18,19	F,F	L,L	382
6	WT DRG	5	1,1,1,1,1	139,51,30,40,38	10,10,10,8,8	M,M,F, F,M	T12,T8,L1,L1,L1	298
	WT Ventral Horn	5	1,1,1,1,1	75,51,23,24,28	10,10,10,8,8	M,M,F, F,M	T12,T8,L1,L1,L1	201
7	WT	2	2	N/A	7,24	M,M	L1,T12	N/A
8	WT	1	1	N/A	7	M	L1	N/A
	Kv2.2 KO	1	1	N/A	7	M	L1	N/A
	MrgprD-GFP	1	1	N/A	13	F	T12	N/A
9	WT	1	1	N/A	28	F	T12	N/A
	Kv2.2 KO	1	1	N/A	28	F	T12	N/A
10	WT	1	1	N/A	10	M	L5	N/A
	MrgprD-GFP	4	6,5,9,14	852,632,842,1392,	13,20,8,8	F,M,F,F	T12,L1,L1,L1	3718
	WT	5	7,4,6,7,4	482,464,592,641,166,	7,10,24,19,19	F,M,M, F,F	L1,T12,T12,T12, T12	2345
	PV-tdTomato	2	15,9	1978,1158,	8,8	F,M	L1,L1	3136
1-1	WT	1	1	N/A	10	M	L5	N/A
1-2	WT	1	1	N/A	28	M	L	N/A

1-3	WT	1	3	125	13	M	L	125
2-1	WT	1	33	5399	8	M	T11 and T12	5399
2-2	MrgprDGFP	1	1	N/A	13	F	T12	N/A
2-3	MrgprDGFP	4	6,15,9,14	5,568,769, 051,487	14,20,8,8	F,M,F,F	L1,L1,L1,L1	3824
	WT	2	7,5	771,478	24,8	M,F	L1,L1	1249
6-1	WT DRG	4	1,1,1,1	25,30,28,3 5	7,7,8	M,F,F,F	L1,L1,L1,L1	118
	WT Ventral Horn	4	1,1,1,1	17,19,26,1 9	7,7,8	M,F,F,F	L1,L1,L1,L1	81
7-1	MrgprDGFP	1	1	N/A	14	F	T12	N/A
	WT	2	1,1	N/A	11,17	M,M	L,L	N/A
8-1	WT	1	1	N/A	7	F	T12	N/A
	Kv2.1 KO	1	1	N/A	7	F	T12	N/A

1282

1283 **Table 1 legend**

1284 Detailed information on mice used in each figure. In columns “Sections/Plates Analyzed”, “ROIs  
 1285 Analyzed”, “Age”, “Sex” and “Level of Spinal Column” information for each mouse is separated  
 1286 by commas. “ROIs Analyzed” corresponds to ROIs generated by automated analysis. In column  
 1287 “Level of Spinal Column” L1 refers to the first lumbar DRG and T12 refers to the twelfth thoracic  
 1288 DRG and if only L is shown the specific DRG is not known but the DRG is from the lumbar  
 1289 region.  
 1290

1291 **TABLE 2**

Antigen	Antibody name	Species/isotype	Manufacturer information	Concentration used	RRID	Figures
Kv2.1	K89/34	Mouse IgG1 mAb	NeuroMab	6.7 ug/mL	AB_10672253	1, 2, 3, 4,6-1, 7, 8-1, 10, 11, 11-1, 11-2
Kv2.2	Kv2.2c	Rabbit pAb	In-house Trimmer laboratory	1:100 purified from strip assay	AB_2801484	3, 4, 6-1, 7, 8, 9, 10, 11, 11-1, 11-2,11-3
Nav1.8	N134/12	Mouse IgG2a mAb	NeuroMab	1:5 tissue culture supernatant	AB_10672261	1,11-1
Kv2.1	K89/34R	Mouse IgG2a mAb	In-house Trimmer laboratory	1:5 tissue culture supernatant	AB_2315768	11-1
beta III Tubulin	NA	Rabbit pAb	Abcam ab18207	0.33 ug/mL	AB_444319	2, 8-1
Kv2.2	N372B/60	Mouse IgG2b mAb	NeuroMab	1 ug/mL	AB_2315868	1, 1-3, 6, 10
NF200	NA	chicken pAb	Abcam ab4680	0.2 ug/mL	AB_304560	3, 8, 10
Caspr	K65/35	Mouse IgG1 mAb	NeuroMab	1:5 tissue culture supernatant	AB_2877274	9
Kv1.2	K14/16	Mouse IgG2b mAb	NeuroMab	1:5 tissue culture supernatant	AB_2877295	9,11
CGRP	NA	Rabbit pAb	Immunostar	1:1000	AB_572217	10
DsRed	NA	Rabbit pAb	Takara Cat#632543	0.17 ug/mL	AB_2307319	10
Nav1.7	N68/6	Mouse IgG1 mAb	NeuroMab	1:5 tissue culture supernatant	AB_2184355	11-1,11-3

1292

1293

1294 **Table 2 legend**

1295 Detailed information on antibodies used throughout the manuscript. In column “Concentration  
 1296 Used” if only dilution is given concentration was unknown however, tissue culture supernatant  
 1297 concentrations of antibodies typically range between 15-30 µg/mL.